Photochemical Processes in Weakly Bound Binary Complexes

MASAO TAKAYANAGI and ICHIRO HANAZAKI*

Institute for Molecular Science, Myodaiji, Okazaki 444, Japan

Received October 31, 1990 (Revised Manuscript Received May 29, 1991)

Contents

I. Introduction

Dynamics of the molecular complexes bound with weak intermolecular forces such as van der Waals forces and hydrogen bonding has recently attracted considerable attention. Among various types of work, the photoinitiated chemical reactions of these complexes are of particular interest since they would extend the research field of chemical reaction dynamics by adding some new features to it.

Among several points of interest, we would particularly emphasize here the following two aspects which seem to be most important and to make the dynamics of these complexes distinct from that of normal molecules. First, this kind of complexes has weak intermolecular bonds which add some characteristic features to their dynamics. It is essential in the study of their dynamics to elucidate how the intermolecular vibrational modes are involved in and characterize the dynamics of relaxation and chemical reaction.

Second, the weakly bound complexes give us an opportunity of investigating the "half reaction" or "half collision", which corresponds to the latter half of a bimolecular collisional process. In bimolecular reactions, the collision parameters such as the relative alignment of reactant molecules, the relative translational energy, and the impact parameter determine a differential cross section. However, in a conventional measurement of reaction rate, one obtains only the integrated cross section as a result of statistical averaging over all possible values of collision parameters. Among several efforts to specify the collision condition to obtain a differential cross section, the hexapole electric field[1-8] and polarized excitation techniques[5-14] have been applied to select a particular relative orientation of reaction partners. Relative translational energy may also be selected by using a crossed molecular beam with velocity selection.[15] However, the impact parameter remains still uncontrollable. By photoexciting the complex corresponding to the reaction intermediate or collision complex in a bimolecular reaction, it is possible in principle to start the reaction with well-defined "collision" parameters (energy, impact parameter, and relative orientation) determined by the geometry of the parent complex. Comparing the results with the corresponding bimolecular collisional process, one could study the dynamics in substantial detail.

In this article, which covers the literature before July 1990, we intend to review the current status of studies on the photoinitiated chemical reaction of the weakly bound binary complexes by trying to give a unified understanding of the phenomena and to survey possible future development of the research field. The materials to be reviewed in this article will be divided into two parts: The rearrangement reactions of the complexes initiated by photoexcitation of one of the constituent molecules to its dissociative excited state[16-36] are discussed in section II, and the rearrangement reactions initiated by the photoexcitation to the bound state of one of the constituents[37-61] are discussed in section III. We shall not discuss here the case where the photoexcited complex dissociates simply into its constituent molecules, since it constitutes another big field of research to be reviewed separately.[62,63] The reactions of complexes initiated by photoionization are also excluded since the discussions have so far been limited to their energetics; neither reaction mechanism on the

0009-2665/91/0791-1193$09.50/0

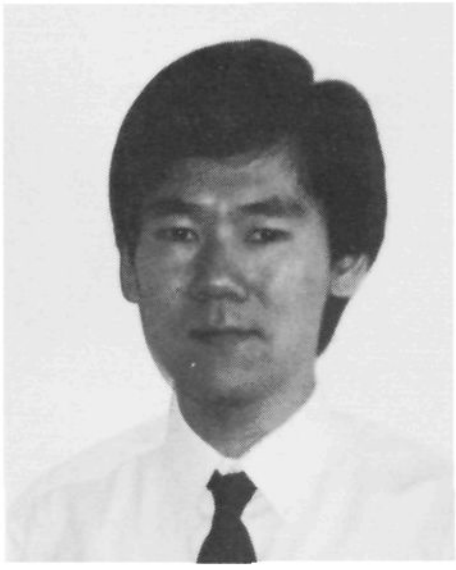

Masao Takayanagi was born in Tokyo, Japan. He graduated from The University of Tokyo in 1982. From 1982 to 1986, he worked with Mitsuo Tasumi at The University of Tokyo, where he studied inverse Raman spectra of fluorescent dyes and the electronically resonant effect on the inverse Raman band shapes, for which he obtained Ph.D. in science in 1989. Since 1986, he has been working as a research associate at Institute for Molecular Science. His main research subjects are dynamics of vibrationally excited molecules and van der Waals complexes in molecular beams as studied by the SEP and SEP-LIF techniques.

Ichiro Hanazaki was born in 1936 in Tokyo, Japan. He graduated from The University of Tokyo, and received his Ph.D. from the same in 1966 for "The Studies on the Electronic Structures of Organic Reaction Intermediates". After working for 6 years as a research scientist at The Institute of Physical and Chemical Research and another 6 years as an associate professor at the department of chemistry, Osaka University, he has been a professor at Institute for Molecular Science since 1978. His scientific interests have been the electronic structure of organic reaction intermediates and metal chelate complexes, and the theory of optical rotatoy power. Topics he is now interested in are: (1) the effect of vibrational excitation on molecular dynamics, including the IR multiphoton process, highly excited local modes, vibrational photodissociation of van der Waals complexes, and application of the stimulated emission pumping technique to the vibrational excitation of molecules; (2) the rearrangement reaction of photoexcited weakly bound binary complexes produced in a molecular beam; (3) the self-organizing chemical reactions including chemical oscillators and spatial pattern formations, and the photoirradiation effect on these systems.

basis of their geometry nor relation with the corresponding bimolecular reactions has been discussed.[64-66]

Comparison of the photoinitiated reaction of the complex in a molecular beam with the corresponding bimolecular reaction in a static (or flow) cell will appear repeatedly throughout this article. In order to avoid possible confusion, we shall hereafter distinguish them by designating the former as the "reactant-pair" reaction and the latter as the "bimolecular" reaction.

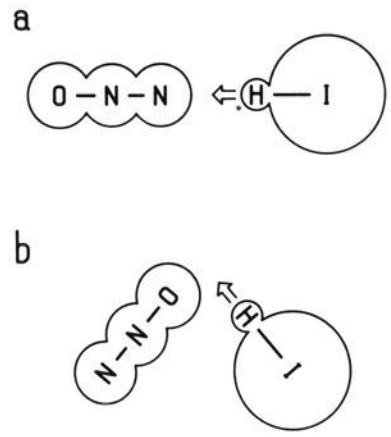

Figure 1. Two conformers expected for $HI \cdot N_2O$. The positions and directions of the attack of hydrogen to N_2O are shown by arrows.

II. Reactions Initiated by Photoexcitation to Dissociative States

A. General Considerations

This type of reactions can be written generally as

$$AB \cdot CD + h\nu \rightarrow (AB)^* \cdot CD \rightarrow A \cdots B \cdots C \cdots D \rightarrow A + BC + D \quad (1)$$

where AB and CD are the constituent molecules and A, B, C, and D may be either molecules or atoms. (AB)* represents AB in its dissociative excited state. The corresponding bimolecular reaction is

$$AB + h\nu \rightarrow A + B$$
$$B + CD \rightarrow B \cdots C \cdots D \rightarrow BC + D \quad (2)$$

where B attacks CD with all possible values of collision parameters.

Let us examine some general features underlying the phenomenon by taking $HI \cdot N_2O$ as an example.[32] The reactant-pair reaction is initiated by the UV photolysis of the complex

$$HI \cdot N_2O + h\nu \rightarrow (HI)^* \cdot N_2O \rightarrow I \cdots H \cdots N_2O \rightarrow I + OH + N_2 \quad (3)$$

In the corresponding bimolecular reaction, which proceeds in a flowing mixture of HI and N_2O, the hydrogen atom generated by the photodissociation of HI attacks N_2O to form OH and N_2 as follows:

$$HI + h\nu \rightarrow I + H$$
$$H + N_2O \rightarrow H \cdots N_2O \rightarrow OH + N_2 \quad (4)$$

Reactions 3 and 4 correspond to reactions 1 and 2, respectively. In both of reactions 3 and 4, the distribution over the rotational states of one of the products, OH, is probed with the LIF (laser-induced fluorescence) technique.

In the bimolecular reaction, the nascent distribution over vibrational and/or rotational states can be obtained by employing a gas pressure of $\sim 10^{-2}$ Torr and a delay time between the photolysis and probe laser pulses of ~ 100 ns. The hydrogen atom generated in this way collides with N_2O randomly, the collisional geometry and the impact parameter being unspecified. Although the relative translational energy of hydrogen with respect to iodine could be determined uniquely by a single-frequency photolysis, the relative energy of hydrogen with respect to N_2O cannot be specified because of the thermal velocity distribution of parent HI and N_2O.

It is possible to produce the complex $HI \cdot N_2O$ in a supersonic expansion of the mixture of HI and N_2O

with rare gases. Although the structure of $HI \cdot N_2O$ is not known, two conformers are expected to exist (Figure 1) by the analogy of $HX \cdot N_2O$ (X = F, Cl, and Br).[67-76] The isomers have different thermodynamical stability and their relative abundance in a supersonic beam can be controlled by varying the stagnation pressure. By irradiation with a UV laser, the HI part of the complex is excited to the state which corresponds to the dissociative excited state of HI. The hydrogen atom then attacks N_2O within a framework of the complex, with the position and direction of attack confined to a narrow range determined by the geometry of the parent complex as indicated by arrows in Figure 1. The "collision" energy in this case is the excess energy carried by the hydrogen atom on the excited potential surface and well defined as the difference of the photon energy and the potential energy. By comparing the results with those of the bimolecular experiment, it is possible to obtain information on the relative importance of two channels, in which the hydrogen atom attacks the terminal oxygen or nitrogen atom of N_2O.

One of the original ideas in the studies of the complex was, as mentioned above, to investigate the corresponding bimolecular reaction under a specified collision condition. For example, one of the first studies of this type was done for $HBr \cdot CO_2$, which was aimed to investigate the bimolecular reaction, $H + CO_2 \rightarrow OH + CO$, with limited collision parameters.[18] It assumed implicitly that the halogen atom played a role *only* in restricting the impact parameter. However, later studies have revealed that this is not the case. The product state distributions are indeed seriously affected by the presence of the halogen atom as discussed in section II.G. Now we believe that the complexes should be studied with interests in their own characteristic dynamics, not as impact parameter limited analogues of bimolecular reactions, although a comparison between reactant-pair and bimolecular reactions can still provide plenty of information on the reaction dynamics of the system.

B. Reaction Mechanism

In the following description of individual systems, discussions of the reaction mechanism based on a comparison of the rotational distributions of a product between the bimolecular and reactant-pair reactions will appear frequently. The discussions given so far in the literature seem to be rather tentative and somewhat confusing. Therefore, it would be relevant to summarize here an outline of the discussion. The discussions are qualitative and more or less based on the classical dynamical model. In Figure 2, a schematic potential curve[77] is given for the bimolecular reaction of H and N_2O. Two channels correspond to the attack of the hydrogen atom at the terminal nitrogen and oxygen atoms:

$$H + NNO \rightarrow H\cdots N\cdots N\cdots O \rightarrow OH + N_2 \qquad (5)$$

and

$$H + NNO \rightarrow H\cdots O\cdots N\cdots N \rightarrow OH + N_2 \qquad (6)$$

The minimum in the center of the potential curve corresponds to the metastable intermediate H···N···N···O. In some cases the intermediate is stable enough to have a lifetime during which the energy can randomize statistically over the internal degrees of freedom. We shall call this case as "indirect". The resultant rotational excitation is determined mainly by the statistical factor. An additional specificity in the distribution, if any, may arise from the shape of potential surface downward to the final products.

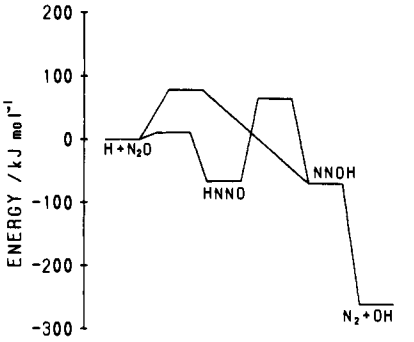

Figure 2. A schematic potential curve for the bimolecular reaction of H and N_2O based on the result given in ref 77. Two channels correspond to the attack of H to the terminal N and O of N_2O.

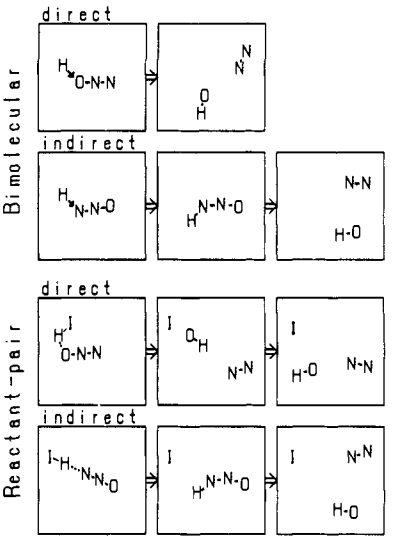

Figure 3. The direct and indirect mechanisms in the bimolecular and reactant-pair reactions.

On the contrary, the "direct" case will be realized if the intermediate has a very short lifetime during which there is no time of energy randomization. An example is reaction 6, where an ab initio calculation[77] has predicted no minimum for H···O···N···N (Figure 2), suggesting this channel to be direct. In this case, the hydrogen atom attacking N_2O with the specific values of collision parameters, which are preferable in view of the cross section, results in a specific distribution of energy over the product internal and translational degrees of freedom. In other words, the system retains its memory of the initial collisional encounter, which determines the distributions over the internal states of the final products. The processes are illustrated in Figure 3 together with those for the reactant-pair case discussed below. It is to be noted that the indirect case will approach the direct case if the relative translational energy becomes much higher than the reaction barrier, since too much energy in the intermediate will make its lifetime shorter. Therefore, the classification into direct and indirect should be taken as the limiting cases.

The indirect case may be defined for the reactant-pair reactions as the departure of the iodine atom at earlier

stage of the reaction leaving the intermediate H···N···N···O (Figure 3). Similar to the bimolecular reaction, the resultant distribution would be governed mostly by a statistical factor if the intermediate has a sufficient lifetime for the energy randomization. The difference from the bimolecular reaction is that there is a possibility of partition of the excess energy into the relative translational energy between the intermediate H···N···N···O and the iodine atom. If most of the energy goes into translation, H···N···N···O would have little excess energy to be used for the internal excitation of the products, resulting in lower rotational and vibrational temperatures compared with the bimolecular reaction. Effect of the partition depends on how the potential surface is repulsive in the entrance channel where H attacks N_2O.

On the other hand, the direct process may be defined for the reactant-pair reaction on the analogy with the bimolecular reaction as an instantaneous dissociation of the photoexcited complex into I + OH + N_2 (Figure 3). Here we ignored the possibility of the existence of a metastable intermediate, I···HO. If it were existent, it should constitute another indirect mechanism. Although the effect of the I···HO interaction after the kick-out of N_2 has been suggested in some systems (see section II.G), it has been considered as "collisions" during the course of escaping of OH from the system[22] rather than the intermediate formation. We have presently no definitive evidence for that "intermediate" I···HO to have a sufficient lifetime for energy redistribution. In the direct mechanism, the direction and position of attacking of H at N_2O are restricted by the geometry of the parent complex and this memory is carried over the whole reaction path. The resultant internal excitation depends on how the parent geometry is favorable for the excitation. The possible interaction between I and OH would cool the rotational motion of OH, and would also affect the relative population of the spin–orbit states of product OH through the interaction between the angular momenta of OH and I (see section II.C).

It is clear from the discussion given here that one cannot specify one of the above mechanisms on the basis of the comparison of rotational or vibrational temperatures between the reactant-pair and bimolecular results, since any mechanism discussed above tends to predict a lower temperature for the former. Additional experimental evidences such as the populations over the spin–orbit fine states and Λ-doublets may serve to specify the mechanism. Theoretical studies on the potential surface correlation and trajectory calculations are also helpful.

C. Fine State Distribution

In the case of OH, the population in the spin–orbit states [$F_1(^2\Pi_{3/2})$ and $F_2(^2\Pi_{1/2})$] and the Λ-doublet states [$A'(\Pi^+)$ and $A''(\Pi^-)$] can be determined experimentally by measuring the LIF intensities for the corresponding rotational branches.[78-82] The F_1/F_2 population ratio, after corrected for the degeneracy, should be unity if the partition to F_1 and F_2 occurs statistically (since the energy difference between corresponding F_1 and F_2 states is very small). Deviation from unity indicates some interaction existent between angular momenta. Experimentally, a statistical distribution has been reported for the OH produced in the HBr·CO_2 reaction[19] (see section II.G.2), whereas higher F_1 over F_2 has been reported for the lower rotational quantum numbers of OH produced in the HI·N_2O reaction[32] (see section II.G.6). It is not unreasonable to assume that the indirect case, where the total angular momentum can distribute among several rotational and orbital angular momenta, would impose a loose restriction on the F_1/F_2 ratio. On the other hand, the direct case would impose a more strict restriction: If the iodine atom is finally in the $^2P_{3/2}$ state, the conservation of angular momentum may prefer the F_1 state of OH. The I···HO interaction mentioned above may also give rise to additional effects. Unfortunately the conservation relation cannot be examined exactly because of ambiguities in the multiply dissociative photoexcited state in HI[83] and in the orbital angular momenta in the final state. However, existence of the I···HO interaction and the preferred $I(^2P_{3/2})$ channel because of its higher excess energy could be a reason for the preference of F_1 to F_2.

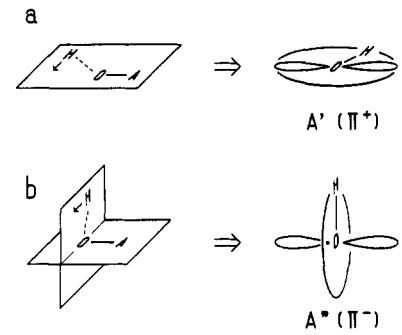

Figure 4. A classical model for the formation of the $A'(\Pi^+)$ and $A''(\Pi^-)$ states of OH. Two extreme cases are illustrated. The hydrogen movement in the H···O–A plane results in the formation of OH in the $A'(\Pi^+)$ state (case a), where the $2p\pi$ electron lobe lies in the plane of molecular rotation. The $A''(\Pi^-)$ state is formed when the hydrogen attacks in the plane perpendicular to the O–A axis (case b). The lobe is perpendicular to the plane of rotation.

The Λ-doublet is the splitting due to the interaction of the spin angular momentum with the rotational angular momentum.[78,79] In the $A'(\Pi^+)$ state, the unpaired electron in a 2p atomic orbital lies in the plane of molecular rotation of OH, whereas it lies out of the plane of rotation in the $A''(\Pi^-)$ state. The partition into A′ and A″ has been discussed qualitatively on the basis of a classical model for which two extreme cases are illustrated in Figure 4. In the direct type reaction, two modes of attack occur with nearly equal probability. Therefore, the reaction would give $A'/A'' \approx 1$ if there is no appreciable anisotropy in the cross section. Even in the reactant-pair reaction, coupling of the translational motion of H toward N_2O with the bending motion of H in various out-of-axis directions would result in $A'/A'' \approx 1$. In the case of the indirect reaction, it is possible that A′ or A″ is preferred according to the conformation of the intermediate and the activated complex. An example for this preference will be given in section II.G.6. Thus examination of the fine state distribution would render an opportunity to specify the reaction mechanism in substantial detail.

D. Time-Resolved Measurements

A time-resolved measurement of the unimolecular decomposition rate has recently become available and has been applied to the HI·CO_2 system.[24,25] A short-

pulse laser decomposes the complex and another short-pulse tunable laser is used to monitor the product OH by the LIF technique. With varying delay between two laser pulses, it is possible to measure the rise time of individual rotational states of OH. Some general features pertinent to this kind of studies will be discussed here in terms of the above-mentioned reaction mechanisms.

Taking $HI{\cdot}CO_2$ as an example, we may consider the direct mechanism following the scheme in Figure 3 as

$$[IH\cdots CO_2]^* \xrightarrow[\tau_1]{} I + OH + CO \quad (7)$$

If one measures the rise time of OH, it corresponds to τ_1, the decay of the photoexcited complex. As discussed in section II.B, a collisional interaction has been postulated between I and OH. This interaction would never affect the time evolution unless intermediate I···HO exists. If it excited, scheme 7 should be written as

$$[IH\cdots CO_2]^* \xrightarrow[\tau_1]{} I\cdots HO + CO \xrightarrow[\tau_2]{} I + OH + CO \quad (8)$$

where two time constants, τ_1 and τ_2, would determine the rise of OH.

The indirect case in Figure 3 can be written as

$$[IH\cdots CO_2]^* \xrightarrow[\tau_1']{} I + HOCO \xrightarrow[\tau_2']{} I + OH + CO \quad (9)$$

where τ_1' or τ_2' determines the rise of OH. For $\tau_2' > \tau_1'$, the rise of OH is determined by τ_2', while τ_1' appears as the initial delay of rise. In the case of $\tau_2' < \tau_1'$, τ_1' will be measured as the rise and τ_2' determines the delay of rise. The measured rise time of OH could, therefore, by any of τ_1, τ_2, τ_1', or τ_2'. When the delay of rise is observed, one could conclude that the reaction proceeds by scheme 9 (or 8). However, it is impossible to determine which of τ_1' and τ_2' corresponds to the rise.

We shall close this section with a few remarks: First, the time-resolved study of the complex, in its present status, can determine the rise time of products (say, OH) but can give only a poor information on the mechanistic aspects. Future development on this line should involve the direct detection of the intermediate so that one could determine which process takes place, as well as the direct measurements of τ_2' and τ_1' as the decay and rise times, respectively, of the intermediate.

Secondly, it is to be noted that the measurement is done near the uncertainty limit. Thus, to retain the spectroscopic resolution to measure, say, individual rotational lines of OH, the pulse width should not be less than ~1 ps. On the other hand, to improve the time resolution further, one has to abandon the spectral resolution. However, an incomplete spectral resolution would make the quantitative analysis very difficult, since the probe laser would cover only a part of the rotational envelope. From this point of view, it is rather desirable to use an ultrashort pulse in the femtosecond range to cover the whole rotational envelope. The direct detection of the intermediate mentioned above will be more seriously restricted by this situation. One would encounter a controversy between the time resolution and the identification of spectroscopically unknown intermediates.

Thirdly, the original idea of the time-resolved measurements was to study the bimolecular reaction with a well-defined starting time. In the bimolecular reaction, even the use of a ultrashort photolysis pulse cannot determine the zero of time, since the dissociated H takes some time before it collides with CO_2 and this time is distributed statistically. On the other hand, the time necessary for H to attack CO_2 within the complex should be negligibly short so that one can define the time of initiation very well. However, as discussed in sections II.A and II.G, it is improper to consider it as a time-domain analogue of bimolecular reactions because of the effect of the I atom. Even in the case of scheme 9, the excess energy carried by intermediate HOCO is not equal to the value for the bimolecular reaction, since a considerable amount of energy would be taken as the relative kinetic energy between I and HOCO.

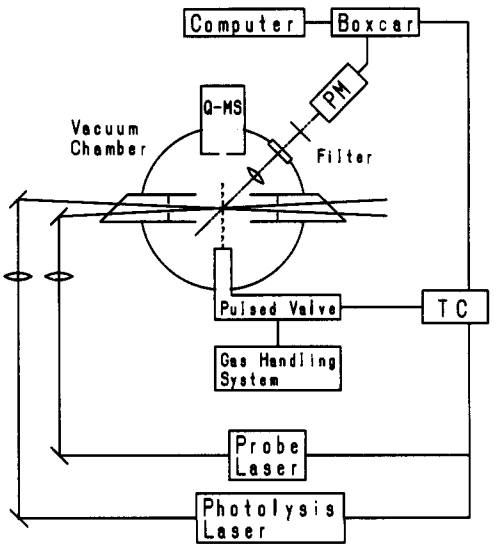

Figure 5. Schematic diagram of a typical apparatus used for the study of the reactant-pair reactions: PM, photomultiplier; Q-MS, quadrupole mass spectrometer; TC, time base circuit.

E. Structural Information

Structural information is important in discussing the mechanism of reactant-pair reactions. The infrared and microwave spectroscopic techniques have recently become available in the molecular beam experiments, which enable us to estimate structures of several weakly bound complexes. However, accumulation of data seems to be still limited and more structural information for a wider variety of complexes are desired. The complexes for which a structural analysis has been reported are summarized in Table I, where we have restricted the systems to those related to the present discussion.[67-76,84-93]

F. Experimental Aspects

1. Equipments and Technique

Details of the equipment used in the studies of the reactant-pair reactions have been discussed in refs 17, 19, 25, and 32. A typical example is illustrated in Figure 5, where a vacuum chamber with a pulsed supersonic beam source is combined with laser sources for excitation and detection. The complex is produced in a chamber by the pulsed supersonic expansion of premixed reactants diluted by rare gas. A mass spectrometer (a quadrupole mass spectrometer in most cases) is

TABLE I. Experimental Studies on the Structures of Complexes

technique	condition	observed structure	year	ref
		N_2O·HF		
electric resonance	mol beam	bent	1981	67
IR	matrix isolated	bent	1981	68
near-IR	mol beam	linear	1987	69
microwave	mol beam	linear	1987	70
IR	mol beam	linear	1988	71
IR	matrix isolated	bent, linear	1989	72
microwave	mol beam	bent	1989	73
microwave	mol beam	bent, linear	1989	74
IR	mol beam	bent, linear	1989	75
IR	mol beam	linear	1990	76
		N_2O·HCl		
IR	mol beam	bent	1990	76
		N_2O·HBr		
IR	mol beam	bent	1990	76
		N_2O·HI		
No experimental datum is available.				
		CO_2·HF		
electric resonance	mol beam	linear	1981	84
IR	matrix isolated	linear	1981	68
microwave	mol beam	quasilinear	1983	85
IR	mol beam	linear	1987	86
IR,microwave	mol beam	quasilinear	1989	87
IR	mol beam	linear	1990	88
		CO_2·HCl		
microwave	mol beam	linear	1982	89
microwave	mol beam	quasilinear	1983	85
IR	mol beam	linear	1990	88
		CO_2·HBr		
IR	mol beam	bent	1990	88
		CO_2·HI		
No experimental datum is available.				
		CO_2·H_2S		
microwave	mol beam	cyclic	1990	90
		OCS·HF		
electric resonance	mol beam	linear	1981	84
microwave	mol beam	quasilinear	1983	85
microwave	mol beam	linear	1985	91
IR, microwave	mol beam	quasilinear	1989	87
		OCS·HBr		
No experimental datum is available.				
		$(N_2O)_2$		
IR	mol beam	slipped-antiparallel	1988	92
IR	mol beam	slipped-antiparallel	1988	93

equipped to measure the cluster-size distribution.

It is a prerequisite in this type of experiment that the reactants do not react without light irradiation, since a premixing of them before the supersonic expansion is necessary. This situation would seriously restrict possible combination of reactant pairs. (However, the reactant pair which undergoes a slow dark reaction could be treated by mixing them just before the nozzle to minimize the dark reaction.[37])

In most experiments reported so far, a fixed-wavelength light source was used for dissociation (266 nm from a Nd:YAG laser, 248 and 193 nm from an excimer laser and the mixing and/or doubling of the Nd:YAG- or excimer-pumped dye laser). Measurements with a tunable photolysis light are desirable to see the effect of excess energy in the photodissociation. Various alignments of photolysis and probe lasers have been employed; e.g., collinear parallel, collinear antiparallel, and perpendicular crossed.

2. Examination of Observed Data

Collisional bimolecular reactions such as reaction 2 may occur even in a molecular beam during the course of expansion. In order to confirm that the product being detected originates from the complex and not from bimolecular reactions, one may perform a cell experiment with the same partial pressure of the component gases as that for the supersonic expansion.[18,19] In refs 18 and 19, where the reaction of HBr·CO_2 are reported, the cell experiment was done for the HBr (0.5%), CO_2 (3%), and He (96.5%) mixture at the total pressure of 0.2 Torr. The molecular beam experiment was done for the same gas mixture at the stagnation pressure of 1500 Torr. They have expected that any possible bimolecular reaction should occur much more efficiently in the cell. If it is not observed, one could exclude the effect of bimolecular reaction in a supersonic expansion. However, this method should be applied carefully since the estimation of "pressure" at the point of observation in the molecular beam is possible only ambiguously. In the above example, the distance of 2.5 cm of the observation point from the nozzle and the nozzle diameter 0.5 mm would give us an order estimation of the pressure at this point to be ~0.15 Torr based on the simple spatial expansion of gas. However, a possible concentration of molecules in the beam direction may give a much higher pressure, while the beam alignment in a unidirection and the low temperature attained in the beam would reduce the number of collisions. Thus the comparison should be taken as only qualitative.

A more direct evidence may be obtained by examining the time evolution of the product signal measured with various delay times between the photolysis and probe pulses. When the products are formed by collision between monomer molecules, the product signal reaches a maximum some time after the irradiation of the photolysis laser. The delay corresponds to the flight time of the hot atom such as H generated by the photolysis pulse to a reaction partner, as observed actually in the cell experiments. On the other hand, no rise time is observed in the reactant-pair reaction in the nanosecond time scale. This is because the reaction partners stay in contact with each other in the complex when the photolysis pulse initiates the reaction.

It is also essential to confirm that the product being detected originates from the 1:1 complex, say XY, since several higher order species are produced in a supersonic expansion and may give rise to the same product as the 1:1 complex. The confirmation may be accomplished by comparing the stagnation pressure dependence of the LIF signal intensity of product and the mass-spectrometric signal due to the $(XY)^+$ ion. The same pressure dependence is expected if the LIF signal is due to the product from the 1:1 complex.

However, one has to be careful about the fact that the electron-impact ionization may produce $(XY)^+$ not only from the 1:1 complex XY but from the dissociative ionization of higher order complexes. To discriminate

TABLE II. Reactions Initiated by Photoexcitation to Dissociative States

reactant	corresponding bimolecular reaction	probed product	wavelength of photolysis, nm	ref
$(N_2O)_2$	$O + N_2O$	NO	193	16,17
$HBr{\cdot}CO_2$	$H + CO_2$	OH	193	18–22, 35,36
$DBr{\cdot}CO_2$	$D + CO_2$	OD	193	23
$HI{\cdot}CO_2$	$H + CO_2$	OH	239,233–263	24–27
DBr·OCS	D + OCS	OD	193	28
$H_2S{\cdot}CO_2$	$H + CO_2$	OH	193	29,36
$HBr{\cdot}N_2O$	$H + N_2O$	OH,NH	193	21,30,31
$HI{\cdot}N_2O$	$H + N_2O$	OH	266	32
$(OCS)_n$		CO,S_2	222–248	33,34

the source of $(XY)^+$, one may measure the time-of-flight signal for the parent ions, $(XY_2)^+$, $(X_2Y)^+$, $(X_2Y_2)^+$, etc., at each mass number. Their rise times are different depending on species. The difference is predominantly due to the different rates of formation during the expansion, since the velocity is all the same for these clusters. If the rise time of $(XY)^+$ is longer than X^+ and Y^+, and shorter than those for higher order complexes, one can be sure that $(XY)^+$ is due to XY. After examining this point, it is possible to conclude that the product LIF signal is due to the 1:1 complex by comparing stagnation pressure dependence of the optical signal with that of the mass-spectrometric signal.

It is also to be noted that the beam divergence and the spatial distribution of species in a supersonic jet vary with stagnation pressure. The difference of the positions of observation for the mass spectrometry and the optical measurement would sometimes make it difficult to compare the stagnation pressure dependences. This effect would be more or less important in the comparison of the optical and mass-spectrometric signals for a free-jet beam, whereas a much better correlation is expected for a well-defined skimmed beam.

G. Individual Reactions

Table II summarizes the reaction systems studied so far. The first observations of the reactant-pair reactions of this type were reported independently by Honma and Kajimoto[16] for $(N_2O)_2$ and by Buelow et al.[18] for $HBr{\cdot}CO_2$ in 1985. Since then several reactant-pair reaction systems have been reported. Among them, $HBr{\cdot}CO_2$, $HI{\cdot}CO_2$, and $H_2S{\cdot}CO_2$ are related to the bimolecular reaction, $H + CO_2 \rightarrow OH + CO$, which has been studied extensively because it is the reverse reaction of an important primary process, $OH + CO \rightarrow H + CO_2$, in combustion.

1. N_2O Dimer

Honma et al.[16,17] reported the production of NO in the 193-nm photolysis of the N_2O dimer. They found that the stagnation pressure dependence of the signal intensity of NO^+ produced by two-photon ionization was the same as that of $[(N_2O)_2]^+$ measured with an electron-impact-ionization mass spectrometer. They also found that the production of NO^+ required three photons in all. On the basis of these findings, the reaction via $O(^1D){\cdot}N_2O$ was proposed:

$$(N_2O)_2 + h\nu\ (193\ \text{nm}) \rightarrow O(^1D){\cdot}N_2O + N_2 \rightarrow 2NO + N_2 \quad (10)$$

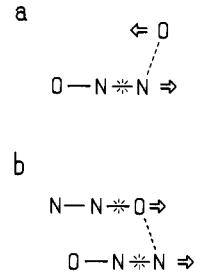

Figure 6. Rotational excitation in the N_2O + O reactin. In the most favorable mode of attack of oxygen to N_2O in the bimolecular case (a), both of the oxygen movement and the dissociation of the N–N bond are summed up to cause the rotational excitation of the product NO, while they are canceled out in the reactant-pair case (b).

LIF measurements for reaction 10 have shown that the vibrational distribution of NO is a superposition of two Boltzmann distributions. The experiment performed with the isotopically labeled reactant $^{15}N^{14}NO$ has shown that the vibrational distributions of ^{15}NO and ^{14}NO are different: ^{15}NO formed from the terminal N and $O(^1D)$ is vibrationally hot, while ^{14}NO is cold. Thus two NO molecules produced in reaction 10 can be discriminated; namely, one formed by the extraction of the terminal nitrogen atom of N_2O in $O(^1D){\cdot}N_2O$ by $O(^1D)$, and the other left after the extraction.

It has also been found that NO produced in reaction 10 is rotationally much colder than that observed in the bimolecular reaction. This result was explained on the basis of the structure of the dimer. In the case of bimolecular collision of $O(^1D)$ and N_2O, the oxygen atom can attack the terminal nitrogen atom of the latter in any direction and with any impact parameter. There should be a set of collision parameters for which the torque due to the attacking $O(^1D)$ and that produced by the N–N bond cleavage can be summed up to excite the rotational motion of product NO (Figure 6a). On the other hand, the slipped parallel geometry of the dimer[92,93] restricts the direction of approach of $O(^1D)$ produced from one of N_2O's to the terminal N of the other so that the torque generated by the attacking $O(^1D)$ and that produced by the N–N bond cleavage cancel each other (Figure 6b). These considerations can explain the difference of the rotational temperatures between the reactant-pair and bimolecular reactions. The geometry of the complex thus specifies the "collision" parameters significantly compared with the corresponding bimolecular collision where a statistical average of reactions with various collision parameters is observed. The effect is reflected fairly sensitively in the internal state distributions of the products.

2. $HBr{\cdot}CO_2$ and $DBr{\cdot}CO_2$

The reactant-pair reaction reported by Buelow et al.[18] and Radhakrishnan et al.[19] is

$$HBr{\cdot}CO_2 + h\nu\ (193\ \text{nm}) \rightarrow OH(X^2\Pi) + CO + Br \quad (11)$$

They have measured the rotational distribution of product OH and have found that OH produced under the reactant-pair condition is rotationally colder than that produced under the bimolecular condition. The results for the R_{11} branch are shown in Figure 7.

They have suggested that the colder rotational distribution may be caused by two dissociation channels

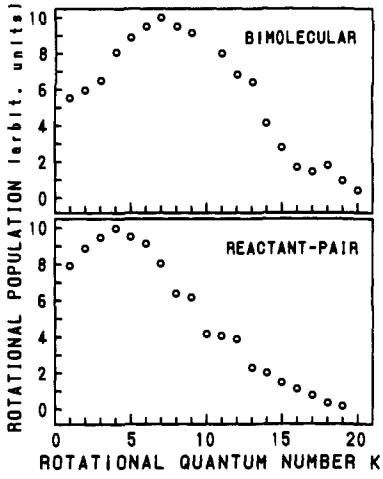

Figure 7. Rotational population for OH in the R_{11} branch obtained in the reaction between HBr and CO_2 under the bimolecular (upper) and reactant-pair (lower) conditions.[35] The figure in the literature was redrawn to make the comparison of data easier.

in the 193-nm photolysis of HBr corresponding to the formation of $Br(^2P_{3/2})$ and $Br(^2P_{1/2})$.[94] The resultant hydrogen atoms have translational energies which are 99% of the available energy [260 and 215 kJ mol^{-1} for the $Br(^2P_{3/2})$ and $Br(^2P_{1/2})$ channels, respectively].[18] The higher energy channel tends to approach the direct case, which has a narrower distribution of differential cross section over collision parameters. If the geometry of the complex is unfavorable for the direct reaction to proceed, the lower energy channel would prevail in the reactant-pair reaction. The lower excess energy would then result in a lower rotational excitation in the reactant-pair reaction.

On the other hand, Wittig et al.[20] have later explained the colder rotational distribution under the reactant-pair condition by the indirect model on the basis of a theoretical analysis (surprisal analysis). They have found that, if the majority of OH produced in the reactant-pair reaction originates from HOCO, its excess energy is estimated to be about 9000 cm^{-1} on the basis of the experimentally determined distribution. It is in contrast to the excess energy of HOCO in the bimolecular reaction which is estimated to be 11 500 cm^{-1}. The departure of Br at an early stage due to the repulsive entrance potential results in a flow of the excess energy into the translational energy between Br and HOCO at the sacrifice of the internal energy of the latter. Another evidence for this point of view has been obtained by the sub-Doppler measurement of the LIF spectra of OH produced from HBr·CO_2 under the bimolecular and reactant-pair conditions.[21] Slightly narrower line widths have been obtained for the latter, indicating that the OH produced under the reactant-pair condition has less kinetic energy than that produced under the bimolecular condition.

A quasiclassical trajectory calculation was made for this reactant-pair reaction by Schatz and Fitzcharles.[22] They assumed a linear equilibrium geometry for HBr·CO_2 and two values of the excess energy, 1.9 and 2.6 eV, corresponding to the formation of $Br(^2P_{1/2})$ and $Br(^2P_{3/2})$, respectively, in the 193 nm photolysis of HBr. The lifetime of intermediate HOCO was estimated to be 0.3 and 0.4 ps at 2.6 and 1.9 eV, respectively. They discriminated two channels for the reaction HBr·CO_2 → Br + OH + CO. One is the indirect channel (a "complex" mechanism in their terminology), in which HOCO moves away from Br before dissociating to OH + CO. The other is the direct channel in which Br and OH interact after CO escapes from the system. Several collisional deactivations of OH by Br were postulated during the course of departure of OH. However, the rotational distribution of OH produced via either mechanism was calculated to be not so much different from those in the bimolecular reaction. The disagreement with the experiments was ascribed to the inaccurate potential surface they employed.

The population ratio of the F_1 and F_2 states of OH was shown to be unity for all rotational states.[19] The ratio of populations in the Λ-doublet components indicates a slight preference of the A′ states in which the unpaired electron is in the plane of molecular rotation.[19] No further discussion has been made on these results.

The deuterium analogue of reaction 11 was also examined by Buelow et al.[23] No remarkable effect of deuteration was observed on the state distributions of OD, excluding a role of the tunneling effect in this reaction.

The structure of HBr·CO_2 has long been believed to be linear on the analogy of HF·CO_2[68,84-87] and HCl·CO_2[85,89] whose structures have been analyzed spectroscopically (see Table I). However, a recent work by Sharpe et al.[88] based on the high-resolution IR absorption spectroscopy has revealed that the equilibrium geometry of HBr·CO_2 is a quasi T-shape with the bromine atom lying ~3.6 Å from the carbon atom along a line perpendicular to the CO_2 axis, and with the H atom somewhere between Br and one of the O atoms. It is therefore necessary to reexamine the previous discussions based on the linear structure.

3. *HI·CO₂*

Chen et al.[26] measured the rotational distribution of OH produced in

$$HI{\cdot}CO_2 + h\nu \rightarrow I + CO + OH \qquad (12)$$

with the photolysis wavelength of 239 nm. The rotational distribution of OH is bimodal and colder than that produced in the corresponding bimolecular reaction. They have assumed the existence of two different excess energies of HOCO, 6000 cm^{-1} (70%) and 800 cm^{-1} (30%), which may be compared with the excess energy of 7880 cm^{-1} for HOCO in the bimolecular reaction. HOCO with the excess energy of 6000 cm^{-1} has been ascribed to the indirect process, where the excess energy is partly taken as the translational energy between I and HOCO. The source of the excess energy of 800 cm^{-1} is not clear, though they have discussed several possibilities. The direct mechanism shown in Figure 3 seems to be most likely where OH loses its rotational energy through the I···HO interaction.

The action spectrum for the photolysis wavelength range of 233–263 nm was measured by probing one of the rotational lines of OH. The quantum yield of the reaction thus determined increases monotonously by increasing the photon energy. They have suggested that higher excess energy gives a more impact-induced deformation of CO_2, resulting in a more stable HOCO intermediate.

Scherer et al.[24,25] reported a time-resolved investigation for this reaction in a picosecond time domain. The photolysis laser was tuned over the range of 231–263

nm, while a properly delayed monitor pulse detected the rise of the $Q_1(1)$ and $Q_1(6)$ lines of OH. An analysis of the temporal behavior led them to ascribe two time constants, τ_1 and τ_2, to the rates of formation and decay, respectively, of HOCO. When the complex is photolyzed at 256 nm, τ_1 and τ_2 are 1.2 and 4.4 ps, respectively, for the OH ($K = 1$) formation. As the photolysis energy increases, τ_2 decreases from 5 ps to 1 ps, while τ_1 is not so sensitive to the energy variation.

Although they assumed the indirect process, their assignment of τ_1 to the rise time of HOCO is suspectable since it was determined indirectly from the rise of OH and is strongly dependent on the model employed in the analysis. They have reported also that τ_2 is shorter for the OH ($K = 6$) formation than for the OH ($K = 1$) formation. This result is inconsistent with what is expected in the RRKM model. They attributed the difference to the effect of the angular momentum constraint. However, it is more likely that these results suggest the process to proceed through a direct mechanism. One should withhold any discussion until direct measurements of the rise time of the intermediate species become possible.

4. $H_2S \cdot CO_2$

The reaction

$$H_2S \cdot CO_2 + h\nu\ (193\ nm) \rightarrow HS + OH + CO \qquad (13)$$

was investigated by Rice et al.[29] They have found that the rotational distributions of OH ($X^2\Pi$, $v'' = 0$ and $v'' = 1$) are extremely colder than those produced in the corresponding bimolecular reaction. On the other hand, the vibrational temperature of OH in the reactant-pair reaction is only slightly colder than that in the bimolecular reaction. The rotational distribution of OH in reaction 13 is even colder than that in the reaction of $HBr \cdot CO_2$.[19] They ascribed the colder distribution in the reactant-pair reaction to the energy partition into the translational degrees of freedom between HS and HOCO in the indirect process. Moreover, in the $H_2S \cdot CO_2$ complex whose equilibrium geometry is cyclic,[90] the hydrogen atom generated by the photodissociation of H_2S may attack CO_2 from its side. This side approach tends to increase the entrance channel barrier to enhance the partition of energy into translation. They tried to explain the colder rotational distribution of OH in the $H_2S \cdot CO_2$ reaction than that in the $HBr \cdot CO_2$ reaction assuming a collinear attack of H to CO_2 in $HBr \cdot CO_2$. However, a more quantitative analysis seems to be required now in view of the recent result of the nonlinear structure of $HBr \cdot CO_2$ mentioned above.[88]

5. DBr·OCS

Haeusler et al.[28] examined the reaction of DBr·OCS:

$$DBr \cdot OCS + h\nu\ (193\ nm) \rightarrow OD(X^2\Pi) + CS(X^1\Sigma) + Br \rightarrow SD(X^2\Pi) + CO(X^1\Sigma) + Br \qquad (14)$$

DBr was used instead of HBr, since SH could not be observed by the LIF technique because of a fast predissociation in the excited electronic state.[95,96]

The heats of formation for the corresponding bimolecular reactions are[28]

$$D + OCS \rightarrow OD(X^2\Pi) + CS(X^1\Sigma)$$
$$\Delta H = 230 \pm 13\ kJ\ mol^{-1}$$

$$D + OCS \rightarrow SD(X^2\Pi) + CO(X^1\Sigma)$$
$$\Delta H = -43 \pm 13\ kJ\ mol^{-1}$$

Comparison of the reaction mechanisms for these two channels is interesting because of a large difference in ΔH value, although both channels are accessible energetically: The deuterium atom generated from DBr by the 193-nm irradiation, $DBr + h\nu \rightarrow D + Br(^2P_{3/2})$, has the translational energy of about 238 kJ mol^{-1} (98% of the available energy, 244 kJ mol^{-1}).[23]

In the corresponding bimolecular reactions, the rotational distribution of OD is statistical, while that of SD is nonstatistical.[28] They have ascribed the former result to the indirect mechanism with a long-lived intermediate for the OD + CS channel, while the extremely high excess energy in the SD + CO channel makes it direct, the distribution being governed nonstatistically by the anisotropy of the reaction cross section.

However, there is another mechanism which could account for the observation: The deuterium atom produced in the process, $DBr + h\nu$ (193 nm) $\rightarrow D + Br(^2P_{1/2})$, has the translational energy of 201 kJ mol^{-1} (98% of the available energy, 206 kJ mol^{-1}),[23] for which the OD + CS channel can hardly occur. The contribution of the $Br(^2P_{1/2})$ channel which leads exclusively to the SD production could make its rotational distribution nonstatistical.

The observation of the reaction under the reactant-pair condition was reported to be very difficult because of the subreactions such as the formation of D_2S in a nozzle. LIF spectra of SD could not be measured at all. Only the rotational distribution of OD was measured for the R_{11} branch with a poor SN ratio, showing a statistical rotational distribution corresponding to the indirect mechanism.

6. $HI \cdot N_2O$

Ohoyama et al.[32] measured the rotational distribution of OH generated from $HI \cdot N_2O$ by the 266-nm laser irradiation (see reaction 3). Boltzmann plots of the experimental results for the R_{11} branch are shown in Figure 8. Rotational distribution observed for the reactant-pair reaction is a superposition of three Boltzmann distributions characterized by the rotational temperatures of 120, 1500, and 4000 K. On the other hand, the OH rotational distribution obtained in the bimolecular reaction is characterized by two Boltzmann distributions with the rotational temperatures of 120 and 4000 K. Relative abundance of these distributions is strongly dependent on the stagnation pressure. It seems to converge to a specific value upon increasing the stagnation pressure, while it approaches to the value in the bimolecular reaction upon lowering the stagnation pressure.

A theoretical study by Marshall et al.[77] for the reaction, $H + N_2O \rightarrow OH + N_2$, has predicted two paths to which the plural Boltzmann distributions may be ascribed; namely, the hydrogen atom attacks the terminal nitrogen or oxygen of N_2O (Figure 2). These channels correspond to two isomers of $HI \cdot N_2O$ mentioned in section II.A. The complex generated with low stagnation pressures is not so cold that the constituents can rotate freely to isomerize between two geometries. The

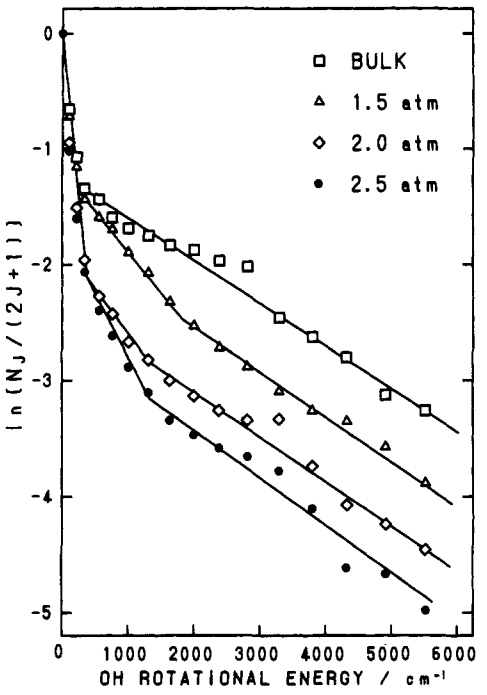

Figure 8. Boltzmann plot for the R-branch rotational distribution of OH obtained in the reaction N_2O + HI under the bimolecular (bulk) and reactant–pair conditions.[32] The results obtained with three different stagnation pressures are shown for the reactant–pair experiment. Each distribution is normalized separately at zero rotational energy.

rotational distribution of OH then approaches the bimolecular result since the hydrogen atom generated from HI attacks N_2O in almost arbitrary directions. On the other hand, with high stagnation pressures, the complex is frozen into either of the two conformers shown in Figure 1. The relative abundance of the conformers is determined by their thermodynamic stability and the transient dynamics during the freezing.

From the analysis of the plural Boltzmann distributions, Ohoyama et al.[32] have assigned the 4000 and 120 K distributions to the N-isomer and O-isomer channels, respectively. Although this assignment accounts for various experimental results and is consistent with the existence of two isomers for HF·N_2O,[67-76] the intermediate distribution of 1500 K remains unassigned. If it is assumed to arise from the N isomer, the ratio of the integrated populations due to the N channel, $[OH]_N$, and to the O channel, $[OH]_O$, is estimated as $[OH]_O/[OH]_N = 0.9$ at the stagnation pressure of 2.5 atm, while it decreases down to $[OH]_O/[OH]_N = 0.11$ for the bimolecular case as the stagnation pressure decreases. Providing that the ratio of the reaction cross sections for two channels, σ_N/σ_O, is common for the bimolecular and reactant-pair reactions, the relative abundance of the O isomer to the N isomer is estimated as [O]/[N] = 8.0 for the stagnation pressure of 2.5 atm, on the basis of the assumption that both isomers are equally existent, [O]/[N] = 1.0, at the low stagnation pressure limit.

On the other hand, if one assumes that the 1500 K distribution arises from the O isomer,[32b] $[OH]_O/[OH]_N$ for the stagnation pressure of 2.5 atm is estimated to be 1.7, and the corresponding ratio [O]/[N] = 15 is obtained. Although the assignment of the 1500 K component is not definitive, Ohoyama et al.[32b] have later concluded that it should be due to the O-isomer channel, since the stagnation pressure dependence of the 1500 K component is similar to that of the 120 K component. The origin of this distribution is, however, still open to question.

They have also determined the ratio of population A′/A″ of Λ-doublet, which is nearly 1 for the reactant-pair reaction but is higher (2–2.5) in the bimolecular reaction. The strong preference of the A′ state formation has been ascribed to the dominant N-channel in the bimolecular reaction, where the cyclic activated complex[77] prefers the formation of OH with its unpaired electron in the plane of molecular rotation of OH (see Figure 4).

The ratio of population in the OH rotational states F_1/F_2 was also determined. The ratio is near unity except for low rotational quantum numbers (K), where it increases up to 4 at $K = 1$. Although the mechanism is not clear enough, the I···HO interaction is presumably effective in the direct O-channel prevailing at lower rotational states. The excess energy for the $I(^2P_{1/2})$ channel of the 266-nm dissociation of HI is almost the same as the potential barrier calculated for H + N_2O → OH + N_2 so that the $I(^2P_{3/2})$ channel would exclusively effective in this reaction. The preference of F_1 at lower K values may be explained on this basis together with the angular momentum conservation. However, they reported also a similar preference of F_1 at lower K even in the bimolecular reaction, which cannot be accounted for by the above-mentioned scheme.

7. *HBr·N_2O*

Hoffmann et al.[30,31] reported the following reactions of HBr·N_2O:

$$\begin{aligned} HBr{\cdot}N_2O + h\nu\ (193\ nm) &\xrightarrow{k_1} OH(X^2\Pi) + N_2(X^1\Sigma) + Br \\ &\xrightarrow{k_2} OH(A^2\Sigma) + N_2(X^1\Sigma) + Br \\ &\xrightarrow{k_3} NH(X^3\Sigma) + NO(X^2\Pi) + Br \end{aligned} \quad (15)$$

The heats of formation for the corresponding bimolecular reactions are[30,31]

$$\begin{aligned} H + N_2O \rightarrow OH(X^2\Pi) + N_2(X^1\Sigma) \quad & \Delta H = -263\ kJ\ mol^{-1} \\ \rightarrow OH(A^2\Sigma) + N_2(X^1\Sigma) \quad & \Delta H = 128\ kJ\ mol^{-1} \\ \rightarrow NH(X^3\Sigma) + NO(X^2\Pi) \quad & \Delta H = 134\ kJ\ mol^{-1} \end{aligned}$$

They measured, for both of the reactant-pair and bimolecular reactions, the vibrational and rotational distributions of nascent $OH(X^2\Pi)$, $OH(A^2\Sigma)$, and $NH(X^3\Sigma)$ by the LIF technique [$OH(X^2\Pi)$ and $NH(X^3\Sigma)$] and by measuring emission spectra [$OH(A^2\Sigma)$]. Following three findings were reported: (i) In the bimolecular reaction, the emission of $OH(A^2\Sigma)$ is so intense that the LIF spectra of $OH(X^2\Pi)$ cannot be measured. On the other hand, the $OH(A^2\Sigma)$ emission is hardly observed under the reactant-pair condition. (ii) $NH(X^3\Sigma)$ is observed in both reactions. The rotational distribution of NH produced in the reactant-pair reaction is found to be slightly colder than that produced in the bimolecular reaction. (iii) The ratio $k_3/k_1 \approx 0.5$ is obtained in the reactant-pair reaction from the LIF signal intensities of $OH(X^2\Pi)$ and $NH(X^3\Sigma)$.

Possible reasons for the lack of the emission of OH($A^2\Sigma$) under the reactant-pair condition were discussed on the basis of (a) a restricted geometry of the complex which is unfavorable for the OH($A^2\Sigma$) channel (the direct mechanism), (b) quenching of OH($A^2\Sigma$) by Br in the direct mechanism, and (c) the loss of excess energy into the translational degree of freedom between Br and H···N_2O (the indirect mechanism). The last reason was thought also to cause the colder distribution of NH($X^3\Sigma$) under the reactant-pair condition. In relation to b, they have also postulated the quenching by N_2. However, the quenching by N_2, which must be equally effective in the bimolecular reaction, is unlikely to cause the difference.

The ratio $k_3/k_1 \approx 0.5$ under the reactant-pair condition seems to be extremely large in view of their ΔH values. Hoffmann et al.[30,31] have explained the result assuming that two isomers, BrH·NNO and NNO·HBr, exist on the analogy of HF·N_2O,[69-75] and that the former is more stable and more abundant. Most of the reactions occur from the former isomer. They have also assumed a loose exit channel of the intermediate HNNO to the transition state for the NH + NO production, while the exit channel from HNNO to OH + N_2 is narrow. The loose channel for the former would give a large integrated cross section and the rate would be higher if the system has sufficient excess energy to overcome ΔH. It is reasonable to assume a narrower channel for the latter, where the activated complex is considered to be cyclic.[77] However, their assumption of more stable N isomer in the reactant-pair case is in contrast to the result obtained for HI·N_2O discussed above.[32] Unfortunately, the HI·N_2O system was studied at 266 nm with no excess energy available for the NH formation. It is desirable to investigate both systems with the same excess energy to clarify this point further.

8. Miscellaneous

Sivakumar et al.[33,34] reported the photodissociation of OCS clusters $(OCS)_n$ (n = 2–8) in the 222–248-nm region. They observed formation of S_2 and measured the rotational distribution of CO with a VUV laser. However, they neither specified the cluster size nor discussed the mechanism from the viewpoint of the initial state defined reaction.

III. Reactions Initiated by Photoexcitation to Bound States

A. General Considerations

1. Reaction Scheme

This type of reactions may be written generally as

$$A\cdot BC + h\nu \rightarrow A^*\cdot BC \rightarrow AB + C \qquad (16)$$

where A may be either a molecule or an atom, although, in the previously reported works, A is confined almost exclusively to atomic species. A* represents the species in its bound excited state. The corresponding bimolecular reaction is

$$A + h\nu \rightarrow A^*$$
$$A^* + BC \rightarrow AB + C \qquad (17)$$

where A* is assumed to have a sufficiently long lifetime to collide with BC.

The product AB may be in either the ground or the electronically excited state. The former can be probed by the LIF technique, while the latter can be probed by measuring a chemiluminescence spectrum. In both cases, the vibrational and rotational state distributions of the product can be determined by analyzing the spectra. Action spectra can also be measured by scanning the pumping light while the product chemiluminescence or LIF is monitored at a fixed wavelength. In contrast to the excitation to dissociative states, it is possible to vary the excitation energy only discretely corresponding to the bound excited states of A.

A characteristic feature of this type of reactant-pair reactions is that it is possible to excite more than one state selectively, which leads to different reaction channels. The excited states are often characterized by the orientation of a p electron in A with respect to the molecular field provided by BC. The reaction cross section and internal energy distribution of the product have been discussed on the basis of this anisotropy of the initially prepared states. On the other hand, the relative orientation is distributed randomly in the case of bimolecular reaction 17 and cannot be studied selectively (see, however, the polarization-selected bimolecular reaction discussed in section III.C.3).

In most of the reactions studied so far, atoms like Hg, alkali earths and rare gases have been used as A. Among them, the most extensively studied are the Hg complexes, the corresponding bimolecular reactions of which are the mercury-photosensitized reactions.[97,98] The rare-gas complexes have been studied in relation to the mechanism of excimer formation.[99-101]

2. Electronic Structures and Their Correlation

It seems to be relevant here to characterize the nature of excited states of the complexes and their correlation to the states of separated A and BC. Figure 9 shows a schematic correlation diagram between the free-atom states in the $(ns)^1(np)^1$ electron configuration and those in the complex with a closed shell molecule under the $C_{\infty v}$ symmetry. To the left are shown the excited electronic states in the free atom with the Russel–Saunders coupling. To the right are shown the states under the symmetry of $C_{\infty v}$ without spin–orbit (SO) interaction. Immediately to the left of the $C_{\infty v}$ states are shown the states split due to a weak SO interaction. To the immediate right of the free-atom states are shown the atomic states perturbed weakly by the $C_{\infty v}$ field with corresponding atomic terms. Conventional state designations are also indicated, where $\tilde{A}$ and $\tilde{B}$ are used for $^3P_1^0$ and $^3P_1^1$, respectively, which are strongly allowed due to the SO mixing with the $^1P_1$ states, while $^3P_0^0$ is designated as $\tilde{a}$ since it is only indirectly mixed with $^1P_1$. In the middle, their correlation is shown, where broken lines indicate the existence of interaction. Numbers in the middle indicate a correspondence with the designations in Hund's case c which have sometimes been used in the literature.[47,78]

It is to be noted that, while the $^3P_1^0$–$^3\Pi_0$ state has a pure Π character irrespective of the extent of atom–$C_{\infty v}$ mixing, the $^3P_1^1$–$^3\Pi_1$ state has a pure Π character only at the limit of strong $C_{\infty v}$ field. As the $C_{\infty v}$ field becomes weaker, it mixes with a $^3\Sigma^+$ state as indicated by a broken line and, at the atom limit, the $^3P_1^1$ state has a character of a 1:1 mixture of Σ and Π. No complication

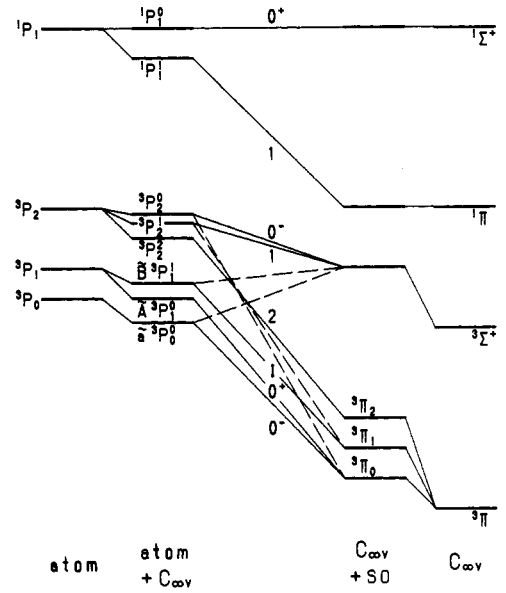

Figure 9. Schematic correlation diagram of the spin–orbit states in a free atom in the $(ns)^1(np)^1$ electron configuration with those in a $C_{\infty v}$ potential due to the complex formation with a closed-shell molecule: (from left to right) free-atomic states with the SO interaction, atomic states split due to a weak $C_{\infty v}$ field, $C_{\infty v}$ states split due to the SO interaction and $C_{\infty v}$ states without the SO interaction. In the middle are indicated their correlation and the Hund's case c designations.

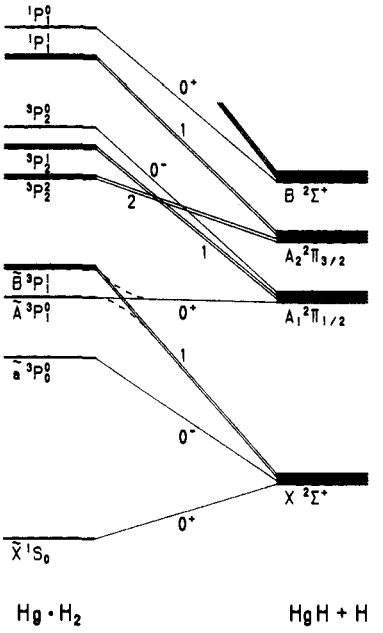

Figure 10. Schematic correlation diagram between Hg·H_2 and HgH + H under the $C_{\infty v}$ symmetry. State designations for HgH + H are those for the HgH molecule.[78] Hund's case c notations are also shown in the middle. Broken curves indicate the avoided crossing under the reduced symmetry of C_s or C_{2v}. Only the correlations between Hg·H_2 and HgH + H are shown. Relative position between the left and right level systems has no significance.

arises for the singlet states. The $^1P_1^0$ and $^1P_1^1$ states correlate with $^1\Sigma^+$ and $^1\Pi$, respectively, independent of the strength of the C_∞ field.

We have assumed a repulsive $C_{\infty v}$ potential in Figure 9, which is the case for most of the known complexes. If it is attractive, the order of the $^3\Pi$ and $^3\Sigma^+$ levels will be reversed and $^3P_1^1$ will be correlated with $^3\Sigma^+$, while $^3P_1^0$ remains correlated with $^3\Pi_0$.

This type of correlation has been confirmed experimentally for the Hg·H_2 complex discussed later[39-47] and several Hg·(rare gas) complexes.[102-110] Although the latter complexes themselves do not undergo any reaction, satellite bands are observed in their LIF spectra on both sides of the $Hg(6^3P_1) \leftarrow Hg(6^1S_0)$ atomic line. One is the $\tilde{A}^3\Pi$ state ($^3P_1^0$–$^3\Pi_0$) appearing in the longer wavelength region of the Hg atomic line and the other is the $\tilde{B}^3\Sigma$ state ($^3P_1^1$–$^3\Pi_1$, $\Pi + \Sigma$ character) in the shorter-wavelength side.

There are two possible ways to accomplish the selection of electron orientation. In the bimolecular reaction, one may use an atomic beam which collides with the target molecules.[13,14] If one defines the principal (z) axis in the direction of the atomic beam, one could selectively excite the $^1P_1^0$ and $^1P_1^1$ states (Figure 9), which are energetically degenerate in a free atom, by lights polarized parallel and perpendicular to the z axis, respectively. If the excited atom collides with the target molecule retaining a $C_{\infty v}$ geometry, the correlation in Figure 9 shows that the parallel and perpendicular excitations create the excited states of symmetry $\Sigma(^1P_1^0$–$^1\Sigma^+)$ and $\Pi(^1P_1^1$–$^1\Pi)$, respectively, corresponding to the p electron orientations in the $C_{\infty v}$ field.

Since the SO interaction in heavy atoms correlates $^1P_1^0$ with $^3P_1^0$ and $^1P_1^1$ with $^3P_1^1$, one can also select $^3P_1^0$ and $^3P_1^1$ by exciting them in a free atom with lights polarized parallel and perpendicular, respectively, to the atomic beam direction. In this case, the parallel and perpendicular excitations lead to the $^3P_1^1$–$^3\Pi_1(\Sigma + \Pi)$ and $^3P_1^0$–$^3\Pi_0(\Pi)$ states, respectively.

The other way of selecting orientation is to excite the states in the complex, where the optically accessible states split into $^3P_1^0$–$^3\Pi_0$ and $^3P_1^1$–$^3\Pi_1$, which can be selected by changing the excitation wavelength. Usually these allowed transitions appear separately around the atomic line ($^3P_1 \leftarrow {}^1S_0$) so that one could select the $^3P_1^0$–$^3\Pi_0$ state (pure Π character) or $^3P_1^1$–$^3\Pi_1$ ($\Sigma + \Pi$ character) states in the $C_{\infty v}$ complex. One could also selectively excite the $^1P_1^0$–$^1\Sigma^+$ and $^1P_1^1$–$^1\Pi$ surfaces, the transitions to which split around the atomic line ($^1P_1 \leftarrow {}^1S_0$). In this case, one can select a state with a pure Σ or Π character.

Figure 10 shows a schematic correlation for the reaction Hg·$H_2 \rightarrow$ HgH + H. The states at the left of the figure are those for Hg·H_2 corresponding to the atom + $C_{\infty v}$ case in Figure 9. The levels at the right are for HgH + H with the state designations for HgH. For example, the ground state corresponds to the doubly degenerate $HgH(X^2\Sigma^+)$ which gives rise to four degenerate states in the HgH + H system. In the middle, their correlation is indicated together with the SO-based notations (Hund's case c). It is to be noted that the $\tilde{a}$ and $\tilde{B}$ states of Hg·H_2 have a $\Sigma + \Pi$ character, correlating to $X^2\Sigma^+$ of HgH + H, while the $\tilde{A}$ state has a pure Π character which correlates to $A_1{}^2\Pi_{1/2}$ of HgH. The $\tilde{B}(1)$ and $\tilde{A}(0^+)$ surfaces therefore cross each other under the $C_{\infty v}$ symmetry. However, the symmetry reduction during the course of reaction due to a rotation of H_2 with respect to Hg may give the minimum energy path. A trajectory calculation based on the ab initio potential surface for the Hg + H_2 system[47] has indicated that the excitation of the $\tilde{A}^3P_1^0$ surface in Figure 10 leads to the rotation of H_2 to form the C_s geometry, where the $\tilde{A}(0^+)$ and $\tilde{B}(1)$ surfaces give rise to an avoided crossing (as

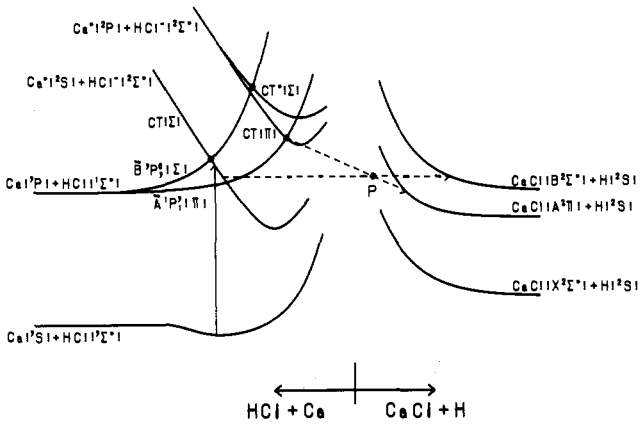

Figure 11. Schematic potential surfaces for Ca + HCl (left half) and CaCl + H (right half). The $C_{\infty v}$ symmetry is assumed to be retained throughout. The Σ and Π surfaces correlating the left half to the right half are indicated by broken lines, which cross each other at point *P*. The crossing would be avoided if the symmetry is reduced to C_s or C_{2v}. Surfaces due to $Ca(^1D)$ and $Ca^+(^2D)$ are not shown since they are not important for the present discussion (see text).

indicated by broken curves in Figure 10). The complex excited to Ã then dissociates into HgH + H (see section III.C.1).

3. The Harpooning Mechanism

Another characteristic mode of reaction is illustrated in Figure 11. These schematic potential energy surfaces show the mode of approach of Ca to HCl keeping the $C_{\infty v}$ symmetry. In the left half of the figure are shown the Ca + HCl surfaces while the right half shows the CaCl + H surfaces. In the left half, the $Ca(^1P)$ + $HCl(^1\Sigma^+)$ surface splits into $\tilde{A}(\Pi)$ and $\tilde{B}(\Sigma)$ on mutual approach. The situation is the same as the splitting of the $^1P_1$ state into $^1\Pi$ and $^1\Sigma^+$ in Figure 9. A characteristic feature in Figure 11 is the incorporation of relatively stable charge-transfer (CT) states in which one of the valence electrons of Ca(sp) is transferred to HCl to form $HCl^-(^2\Sigma^+)$. These CT surfaces are more stable for shorter bond distances and would cross the repulsive neutral surfaces at some distances. Among the two surfaces, $Ca^+(^2S)$ + HCl^- and $Ca^+(^2P)$ + HCl^-, the former crosses the B̃ surface at a larger distance since it contains the process Ca(sp) → Ca^+(s) + e which occurs at lower energy than Ca(sp) → Ca^+(p) + e. The $Ca^+(^2S)$ + HCl^- surface has a Σ symmetry and interacts only with the B̃ neutral surface. On the other hand, the $Ca^+(^2P)$ + HCl^- surface splits into Σ and Π which interact with B̃ and Ã, respectively, as indicated by filled circles. Correlation between the left and right levels are indicated by broken lines, where the CT(Σ) surface correlates with CaCl(B) + H and the CT(Π) surface correlates with CaCl(A) + H under the $C_{\infty v}$ symmetry. If a symmetry reduction (say, $C_{\infty v} \rightarrow C_s$) occurs during the reaction, two surfaces indicated by the broken lines would mix each other at the crossing point P and the Π/Σ selectivity would be lost.

The Ca + HCl system gives the $Ca(^1D)$ + $HCl(^1\Sigma^+)$ and $Ca^+(^2D)$ + $HCl^-(^2\Sigma^+)$ states in addition to those shown in Figure 11. The former locates slightly lower than the $Ca(^1P)$ + $HCl(^1\Sigma^+)$ surface and the latter locates in the middle of the $Ca^+(^2S)$ + $HCl^-(^2\Sigma^+)$ and $Ca^+(^2P)$ + $HCl^-(^2\Sigma^+)$ surfaces. Both are ignored in the figure for the sake of clarity since they are not important for the present discussion. The $Ca^+(^2D)$ + $HCl^-(^2\Sigma^+)$ surface splits into Σ, Π, and Δ surfaces on mutual approach of Ca^+ and HCl^- and the former two could interact with the neutral Σ and Π surfaces, respectively. However, their interactions are governed by a two-electron repulsion such as $\langle 3d4p|4s\varphi^* \rangle$, where φ^* is the antibonding molecular orbital of HCl^-, which should be much smaller than those in the case of the mixing of the $Ca^+(^2S)$ + $HCl^-(^2\Sigma^+)$ or $Ca^+(^2P)$ + $HCl^-(^2\Sigma^+)$ surfaces with the neutrals, where the interaction is governed by the one-electron integral of the type of $\langle 4p|\varphi^* \rangle$ or $\langle 4s|\varphi^* \rangle$.

In the case of bimolecular reaction, if one selects either of the Ã or B̃ surfaces with polarized excitation, the system would slip into the corresponding CT surfaces on mutual approach which are correlated with the CaCl + H surfaces in the right panel.[13,14] In particular, the CT(Σ) surface crosses B̃ at a considerably long distance and correlates with the $CaCl(B^2\Sigma^+)$ + $H(^2S)$ surface without activation barrier. In terms of a classical model, a charge transfer occurs at a considerably long intermolecular distance and the formation of CaCl + H is promoted through the strong attractive force between Ca^+ and HCl^-. It is known as the "harpooning" mechanism[111,112] in which the transferred electron acts as a harpoon to draw the "whale" HCl toward Ca. As a result of a long "shooting range", the reaction could have an extraordinarily large cross section.

Similar to the systems shown in section III.A.2, the photoexcitation of the complex such as Ca·HCl could produce the Ã and B̃ states selectively, which would allow us to study the channel selectivity depending on the p electron orientation in two states. A similar selection of the split components is possible also for the states arising from atomic $^3P_1$ states, as discussed below for $Hg{\cdot}Cl_2$. Unfortunately, only one of the split components has so far been observed in both cases (see sections III.C.3 and III.C.4).

4. Additional Remarks

In some examples discussed below, vibrational structures due to the intermolecular stretching and bending motions have been observed in the excitation and/or action spectra. Excitation of the intermolecular vibration seems to be interesting in view of its role in varying the intramolecular "collision" parameters.

The photoexcited complex, A*·BC, in reaction 16 has often been considered to be identical with the collision complex in reaction 17. Photopreparation of A*·BC is then considered to be a precious technique to access the intermediate state of the bimolecular reaction and to study the latter half of reaction 17. It must be noted, however, that reaction 17 does not necessarily proceed via A*·BC: One should be careful in applying this kind of comparison between reactions 16 and 17. The reactions of complexes of this type, as well as those discussed in section II, should be studied from the viewpoint of their own characteristics, and should not be treated only as the special limiting case of bimolecular reactions.

B. Experimental Aspects

The apparatus used is more or less similar to the one described in section II.F. The only characteristic feature here is the method to obtain sufficient vapor

TABLE III. Reactions Initiated by Photoexcitation to Bound States

reactant	excited state	products	ref
$Hg{\cdot}Cl_2$	$Hg(^3P_1){\cdot}Cl_2$	HgCl(B) + Cl	37–39
$Hg{\cdot}H_2$	$Hg(^3P_1){\cdot}H_2$	HgH(X) + H	39–47
$Xe{\cdot}Cl_2$	$Xe(^3P){\cdot}Cl_2$	XeCl(B,C) + Cl	39,48–50
$Xe{\cdot}Br_2$	$Xe(^3P){\cdot}Br_2$	XeBr(B) + Br	50,51
Ca·HCl	$Ca(^1P){\cdot}HCl$	CaCl(A,B) + H	42,52,53
$Hg{\cdot}N_2$	$Hg(^3P_1){\cdot}N_2$	$Hg(^3P_0) + N_2$	45,54–58
$Hg{\cdot}CH_4$	$Hg(^3P_1){\cdot}CH_4$	$Hg(^3P_0) + CH_4$	56,59
$Hg{\cdot}C_2H_6$	$Hg(^3P_1){\cdot}C_2H_6$	$Hg(^3P_0) + C_2H_6$	56
Hg·CO	$Hg(^3P_1){\cdot}CO$	$Hg(^3P_0)$ + CO	56
$Hg{\cdot}NH_3$	$Hg(^3P_1){\cdot}NH_3$	$Hg(^3P_0) + NH_3$	60,61

pressure of metals such as Hg and Ca, which is very low at the room temperature. A pair of heated source and nozzle (100–120 °C) has been used for the production of Hg vapor,[43,58] while the laser vaporization technique[42,113] has been applied to Ca.

C. Individual Reactions

The systems reviewed here are summarized in Table III. In the following discussion on individual systems, $Hg{\cdot}H_2$ behaves according to reaction 16, while the Hg complexes with other smaller molecules such as N_2, CO, CH_4, and NH_3 show only a simple dissociation into the components. However, the intramultiplet relaxation between the SO components, $Hg(6^3P_1) \rightarrow Hg(6^3P_0)$, has been observed in addition to the channel producing $Hg(6^1S_0)$ and discussed in relation to the excitation-mode selectivity. Since this process has a close relation to the topics being reviewed here, we shall add a brief discussion on this type of systems in section III.C.2. The $Hg{\cdot}Cl_2$, Ca·HCl, $Xe{\cdot}Cl_2$, and related systems have been known to react following the harpooning mechanism discussed above.

1. $Hg{\cdot}H_2$

The reaction of this complex was investigated by Jouvet et al.[39-42] and Breckenridge et al.[43-46] The optical excitation at a frequency near the atomic transition $6^3P_1 \leftarrow 6^1S_0$ of Hg (~250 nm) gives $HgH(X^2\Sigma^+)$ as

$$Hg(6^1S_0){\cdot}H_2 + h\nu \rightarrow Hg(6^3P_1){\cdot}H_2 \rightarrow HgH(X^2\Sigma^+) + H \quad (18)$$

The product can be detected by the LIF technique using the HgH (A ← X) transition. The most important finding for this reaction is that, as shown in Figure 12b, the action spectrum, measured by varying the pump wavelength ($h\nu$) and monitoring the LIF intensity of a particular vibronic band in the HgH (A ← X) transition, is different for the excitation of the $\tilde{A}$ and $\tilde{B}$ states of $Hg{\cdot}H_2$ (see Figure 10), where $\tilde{A}$ and $\tilde{B}$ states are often designated in the literature by $^3\Pi$ and $^3\Sigma$, respectively.

The action spectrum in the $\tilde{A}$ region shows a featureless broad band spreading over 50 cm^{-1}. The lifetime has been estimated to be less than 0.1 ps, assuming that the bandwidth is due to the reactive decay. On the other hand, in the $\tilde{B}$ region at shorter wavelength than the atomic line, two bands are observed, which have been assigned to the 0 ← 0 and 1 ← 0 bands of the intermolecular stretching mode of $Hg{\cdot}H_2$. On the basis of the bandwidth and of the experimental result that no fluorescence is observed for $Hg{\cdot}H_2$ itself, the lifetime of $Hg{\cdot}H_2(\tilde{B})$ due to the dissociation to HgH + H has been estimated to lie between 2 ps and 1 ns. Both of

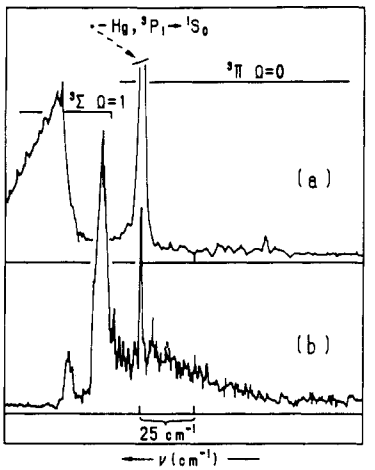

Figure 12. Fluorescence excitation spectrum (a) and action spectrum (b) of $Hg{\cdot}H_2$.[39] Action spectrum was obtained by detecting the probe-laser-induced fluorescence of HgH.

the rotational distributions of HgH ($v'' = 0$) produced by exciting $Hg{\cdot}H_2(\tilde{A})$ and $Hg{\cdot}H_2(\tilde{B})$ are sharply peaked at $N = 19$. The latter has, however, an additional distribution at lower N.

In the LIF spectrum of $Hg{\cdot}H_2$, only a broad structureless band is observed in the shorter wavelength region[39-45] (Figure 12a). This is not due to the emission of $Hg{\cdot}H_2$ but is due to the $^3P_1 \rightarrow {}^1S_0$ emission of the $Hg(^3P_1)$ atom generated by the dissociation of the complex at excitation energies exceeding the dissociation limit in the excited electronic state. The observed spectrum is therefore considered to be the $Hg(^3P_1)$ action spectrum.

These experimental results would provide an opportunity to study the orbitally selective photochemistry. The ground-state potential surface for Hg + H_2 is repulsive except for the weak van der Waals attraction.[47] Similar repulsive potentials have also been suggested for some other metal·H_2 complexes.[114-117] The magnitude of the observed splitting between the $\tilde{A}$ and $\tilde{B}$ states is similar to that in the Hg·(rare gas) complexes.[102-110] The interaction between Hg and H_2 is, therefore, not so strong and should correspond to the "atom + $C_{\infty v}$" case in Figure 9. One of the optically accessible states $\tilde{A}$ corresponds to $Hg(^3P_1^0)$ with a pure Π character in linear $Hg{\cdot}H_2$, whereas $\tilde{B}$ corresponds to $Hg(^3P_1^1)$ with a strongly mixed Σ + Π character.

The experimental results indicate that $Hg{\cdot}H_2$ in the $\tilde{A}$ state reacts very efficiently to form HgH + H. Figure 10 shows that $\tilde{A}(^3P_1^0)$ is correlated not to HgH(X) + $H(^2S)$ but to the $HgH(A_1)$ + $H(^2S)$ surface. However, as discussed in section III.A.2, surfaces $\tilde{A}$–$A_1(0^+)$ and $\tilde{B}$–X(1), which do not mix each other under the exact $C_{\infty v}$ symmetry, interact with each other to give an avoided crossing if the symmetry is reduced slightly into C_s or C_{2v} as indicated by broken curves in Figure 10. The $\tilde{A}(^3P_1^0)$ surface can then be correlated to the ground-state HgH(X) + $H(^2S)$. The trajectory calculation has indicated that the reaction through the C_s symmetry is such that the Hg atom intervenes the H–H bond.[47] No activation barrier exists for this process, accounting for the rapid dissociation observed for the $\tilde{A}$ excitation. Moreover, a calculation taking account of the angular momentum conservation has shown that the rotational distribution of HgH should be peaked at $N = 19$, in exact agreement with experiments.[47]

The $\tilde{B}(^3P_1^1)$ state is strictly degenerate under the $C_{\infty v}$ symmetry not only for Hg·H_2 but also for HgH + H and is correlated to the ground state HgH(X) + H(^{2}S). The trajectory calculation has shown that the $\tilde{B}$ state also has a channel which avoids a barrier by taking a C_s or C_{2v} geometry. In this geometry, a nonadiabatic transition from the $\tilde{B}(^3P_1^1)$–A_1 surface to the $\tilde{A}(^3P_1^0)$–X surface occurs near the crossing point in Figure 10, after which the trajectory will be the same as that for the $\tilde{A}$ excitation. This explains the observation that the main rotational distribution of HgH(X) is the same for the $\tilde{A}$ excitation as for the $\tilde{B}$ excitation. The calculation has shown that there is an additional reaction path which retains the $C_{\infty v}$ symmetry. It has a low activation barrier which could be overcome by the tunneling effect of H. This may account for the additional low-temperature rotational distribution of HgH(X) observed in the $\tilde{B} \leftarrow \tilde{X}$ excitation, since the reaction retaining the $C_{\infty v}$ symmetry would cause little rotational excitation.

Several reaction channels leading to the production of Hg(6^3P_0) + H_2, Hg(6^1S_0) + H_2, and Hg(6^1S_0) + H + H are expected in addition to the production of HgH + H. The latter two are dark channels and have not been studied. The production of Hg(6^3P_0) + H_2 is the dissociation accompanied by a intramultiplet relaxation between the SO components. A trial to detect Hg(6^3P_0) in the dissociation of Hg(6^3P_1)·H_2 by observing the Hg(7^3P_1) → Hg(6^3P_2) emission induced by the Hg(7^3P_1) ← Hg(6^3P_0) excitation was unsuccessful.[43] Branching into this dissociation process was found to be smaller by at least 3 orders of magnitude than that into the dissociation to HgH + H.

2. Dissociation Accompanied by Intramultiplet Relaxation

When complexes Hg·X, where X is a small molecule such as N_2 and NH_3, are excited to the $\tilde{A}$ or $\tilde{B}$ state, correlated to 6^3P_1 of Hg, both of the radiative decay to the ground state and the dissociation into Hg(6^3P_0) + X are observed:

$$\mathrm{Hg}(6^3P_1)\cdot\mathrm{X} \rightarrow \mathrm{Hg}(6^1S_0)\cdot\mathrm{X} + h\nu \quad (19)$$

$$\mathrm{Hg}(6^3P_1)\cdot\mathrm{X} \rightarrow \mathrm{Hg}(6^3P_0) + \mathrm{X} \quad (20)$$

The former can be probed by the fluorescence or LIF measurements, while the latter is a dissociation into the constituents accompanied by an intramultiplet relaxation between the SO components of Hg, which can be probed by the Hg(6^3P_0) action spectra. Since Hg(6^3P_0) is not fluorescent, it has been probed by the Hg(7^3P_1) → Hg(6^3P_2) fluorescence induced by the Hg(7^3P_1) ← Hg(6^3P_0) excitation.

According to the theoretical treatment by Jouvet and Beswick,[54] the anisotropy of the atom–diatom intermolecular interactions opens a route for predissociation accompanied by an intramultiplet relaxation, which is forbidden in the atom–atom cases.

Several complexes containing Hg have been studied experimentally. In both of LIF and action spectra of Hg·N_2[45,55-58] and Hg·CH_4,[56,59] the $\tilde{A} \leftarrow \tilde{X}$ and $\tilde{B} \leftarrow \tilde{X}$ transitions are observed. Both transitions consist of progressions due to the intermolecular stretching and bending vibrations. The widths of the bands have been ascribed to rotational contours. Among the vibrational progressions in the $\tilde{A}$ state region of the Hg(6^3P_0) action spectra of Hg·N_2 and Hg·CH_4, the bands due to the intermolecular bending mode are dominant, while the LIF spectra show structures due to the stretching vibration. The fluorescence lifetime becomes shorter as the complex is excited to higher rotational states in a vibrational band.

The mode dependence has been discussed on the basis of a group theoretical consideration.[56] Under the assumption of C_{2v} equilibrium geometry, the $^3P_1$ atomic level splits into $\tilde{A}(^3A_1)$, and $\tilde{B}(^3B_1$ and $^3B_2)$, while $^3P_0$ becomes $\tilde{a}(^3A_2)$. An A_2-type perturbation is required to induce a nonradiative transition between the $\tilde{A}^3A_1$ and $\tilde{a}^3A_2$ states. Such perturbations can be given (i) by the rotation of the whole system about the principal axis, and (ii) by the combination of the bending vibration (b_1) and the rotation of the whole system about the axis perpendicular to the principal axis (b_2). Although Hg·N_2 and Hg·CH_4 may be in the $C_{\infty v}$ and C_{3v} configurations, respectively, almost the same discussion is valid; the bending motion coupled with rotation has been predicted to be effective in the nonradiative transition between the $\tilde{A}$ and $\tilde{a}$ states, in good agreement with observations. In contrast to the $\tilde{A}$ state, the $\tilde{B}$ state was considered to be unable to interact with the $\tilde{a}$ state directly because of a large energy separation. The two-step process via the $\tilde{A}$ state has been postulated for the $\tilde{B} \rightarrow \tilde{a}$ relaxation.[56]

In the above-mentioned discussions, the geometry of the complex has been assumed not to change during the relaxation process. It has been pointed out,[58] however, that the equilibrium geometries of Hg·N_2 in the $\tilde{X}$ and $\tilde{A}$ states are T-shaped and linear, respectively (the equilibrium geometry is not known for the $\tilde{a}$ state). The relaxation mechanism should be discussed, taking account of the geometry change.

The excited-state dependence of the branching ratio has been observed more clearly for Hg·NH_3, whose excited electronic state has a character of excimer.[60,61] The $\tilde{B}$ state is nonfluorescent and the predissociation to Hg(6^3P_0) + NH_3 is observed exclusively. The rate of the predissociation should be faster than the radiative decay, but slow enough for the structure to be observed in the action spectra. On the other hand, when the complex is excited to a member of the intermolecular stretching progression in the $\tilde{A} \leftarrow \tilde{X}$ band, the radiative decay predominates while the Hg(6^3P_0) formation provides only a minor deactivation route. The bending mode excitation in the $\tilde{A}$ state leads again to only the predissociation to Hg(6^3P_0) + NH_3.

It has been proposed that the selectivity is determined by the presence of angular momentum along the complex axis, which would enhance the $^3P_1$–$^3P_0$ coupling.[61] Since the $\tilde{A}$ state belongs to A_1 under the C_{3v} symmetry of Hg·NH_3, no angular momentum is expected for the intermolecular stretching mode which is of a_1 symmetry, whereas the bending motion, which is of e symmetry, should contribute vibrational angular momentum to the $\tilde{A}$ state. On the other hand, the $\tilde{B}$ state is of E symmetry, which has an electronic angular momentum along the complex axis. Although the reason has not been given clearly why the existence of angular momentum is effective in the coupling, it seems to be evident that this angular momentum coupled with rotational angular momentum gives rise to a nonvanishing matrix element for the $^3P_1$–$^3P_0$ coupling. In this sense, this model seems to be not inconsistent with

those based on purely group theoretical considerations discussed above.

Two anomalously weak bands (tentatively assigned to $v' = 21$ and 23) are observed in the stretching progression in the $\tilde{A}$-state LIF spectrum. The fluorescence lifetime for the bands is less than 30 ns, which is much shorter than 200 ns observed for the other bands. In the action spectra, these two bands are intense compared with the other bands. It has been concluded that the predissociation to $Hg(6^3P_0) + NH_3$ is enhanced for these bands by an accidental level crossing with rovibronic levels in the $\tilde{a}$ state.[61]

The LIF and action spectra of $Hg{\cdot}C_2H_6$ are different from those of $Hg{\cdot}CH_4$.[56] In the $\tilde{A} \leftarrow \tilde{X}$ region, the LIF spectrum exhibits a diffuse spectral feature, while the action spectrum for $Hg(6^3P_0)$ shows a vibrational progression with a spacing of about 80 cm^{-1} in addition to a broad background. In the $\tilde{B} \leftarrow \tilde{X}$ region, an intense diffuse band whose width is 12 cm^{-1} with an underlying broad band is observed in both of the LIF and action spectra. The similarity between the LIF and action spectra in the $\tilde{B} \leftarrow \tilde{X}$ region indicates weak wavelength dependence of the quantum yield for the $Hg(^3P_0)$ production. Existence of conformational isomers were considered to be responsible, at least partly, for the broad bands and spectral congestion. Dissociation of the $\tilde{A}$ and $\tilde{B}$ states of $Hg(6^3P_1){\cdot}C_2H_6$ to $Hg(6^3P_0) + C_2H_6$ with high efficiency was postulated on the basis of their short fluorescence lifetime (less than 1 ns). This view is consistent with the effective quenching of $Hg(6^3P_1)$ to $Hg(6^3P_0)$ and $Hg(6^1S_0)$ by C_2H_6 observed in a static gas experiment.[118]

In the static gas phase, the electronic relaxations, $6^3P_1 \rightarrow 6^3P_0$ and $6^3P_1 \rightarrow 6^1S_0$, of Hg induced by the collision with CO occur with nearly the same efficiency.[118,119] In the $\tilde{A} \leftarrow \tilde{X}$ region of Hg·CO, the LIF and action spectra show a diffuse band.[56] In the $\tilde{B} \leftarrow \tilde{X}$ region, the LIF spectrum exhibits another diffuse band, while the corresponding band has not been observed in the action spectrum. The diffuse bands were attributed to the transitions between the strongly bound excited states ($\tilde{A}$, $\tilde{B}$, and $\tilde{a}$) and the almost repulsive ground state. The intensities in the LIF and action spectra of Hg·CO are very low, lower than those of $Hg{\cdot}N_2$ by a factor of 10, suggesting additional quenching processes such as the nonradiative deactivation to the ground state of the complex.

3. Ca·HCl

In the bimolecular reaction of electronically excited Ca with HCl, two chemiluminescence bands due to the $A \rightarrow X$ and $B \rightarrow X$ transitions of CaCl are observed. $Ca(^1P)$,[13,14] $Ca(^3P)$,[120,121] and $Ca(^1D)$[120-122] have been used as the optically prepared excited atoms. Among them, $Ca(^1P)$ reacts with HCl as follows:

$$Ca(^1S_0) + h\nu\ (422.6\ nm) \rightarrow Ca(^1P_1)$$

$$Ca(^1P_1) + HCl \rightarrow CaCl(A^2\Pi, B^2\Sigma^+) + H$$

$$CaCl(A^2\Pi, B^2\Sigma^+) \rightarrow CaCl(X^2\Sigma^+) + h\nu\ (\sim 600\ nm) \quad (21)$$

Effect of polarized excitation of Ca was investigated under a beam-gas condition by Rettner and Zare,[13,14] who used the excitation polarized parallel or perpendicular to the Ca beam axis to select the $^1P_1^0$ or $^1P_1^1$ excited state of Ca, respectively (see Figure 11 and discussion in section III.A.3). Upon mutual approach of Ca and HCl, $^1P_1^0$ and $^1P_1^1$ split into $\tilde{B}(\Sigma)$ and $\tilde{A}(\Pi)$. The production of $CaCl(A^2\Pi)$ is enhanced when the $\tilde{A}$ surface is selected by polarization perpendicular to the beam direction, while the production of $CaCl(B^2\Sigma^+)$ is favored by the parallel approach along the $\tilde{B}$ surface. Thus the branching into the $CaCl(A^2\Pi)$ and $CaCl(B^2\Sigma^+)$ states depends strongly on the direction of approach to the unpaired electron in a 4p atomic orbital of Ca. On the basis of the harpooning mechanism (Figure 11), the $\tilde{B}$ surface crosses $CT(\Sigma)$ at the very beginning of the entrance channel, corresponding to a large cross section (~ 27 Å^2). The system then moves on the $CT(\Sigma)$ surface which is correlated with $CaCl(B^2\Sigma^+)$. The system selectively excited to $\tilde{A}$ meets the crossing with $CT(\Pi)$ at shorter distance and moves on the $CT(\Pi)$ surface to form $CaCl(A^2\Pi)$.

The photoinitiated reaction of Ca·HCl reported by Jouvet et al.[42] and Visticot et al.[52] is their chemiluminescence spectra obtained by exciting near the resonance line of Ca (430 nm) show two bands corresponding to the $A \rightarrow X$ and $B \rightarrow X$ transitions of CaCl, similarly to the beam-gas experiment. In a later study, a structured action spectrum was obtained by detecting chemiluminescence from the A state of CaCl, which might be due to the $\tilde{A}$ and $\tilde{B}$ excitation of Ca·HCl.[53]

$$Ca{\cdot}HCl + h\nu \rightarrow Ca{\cdot}HCl(\tilde{A},\tilde{B}) \rightarrow CaCl(A^2\Pi, B^2\Sigma^+) + H \quad (22)$$

However, both of the CaCl(A) and CaCl(B) chemiluminescences were observed again by exciting Ca·HCl at 23 750 cm^{-1}, which corresponds to the peak of the A-state action spectrum.[53] This observation shows that both of the A and B states of CaCl are produced from a common excited state of Ca·HCl. Although the discussion given in the literature[42,52] is not clear, the most probable candidate for the "common" origin is the direct excitation of the CT surface, $Ca^+(^2S) + HCl^-(^2\Sigma^+)$, as indicated by a vertical arrow in Figure 11. This surface is correlated with $CaCl(B^2\Sigma^+)$ as indicated by a broken line, but not with $CaCl(A^2\Pi)$ under the strict $C_{\infty v}$ symmetry. However, as discussed previously, a slight deviation of geometry from $C_{\infty v}$ to C_s would cause an avoided crossing between one of the two degenerate components of the $CT(\Pi)$ surface and the $CT(\Sigma)$ surface at P in Figure 11. Therefore, the system excited to $CT(\Sigma)$ would produce both CaCl(A) and CaCl(B) in a fixed ratio. Then, why is the $\tilde{A}$ state not observed in the action spectrum? The most probable answer would be that the $\tilde{A} \rightarrow CT(\Pi) \rightarrow CaCl$ channel has an activation barrier near the crossing point of $\tilde{A}$ and $CT(\Pi)$, which cannot be overcome with the excess energy given by the excitation of $\tilde{A}$. The direct excitation of $CT(\Pi)$ at shorter wavelengths would provide an opportunity to observe this channel.

4. Hg·Cl$_2$

Jouvet and Soep[37] reported the reactant–pair reaction for $Hg{\cdot}Cl_2$ in 1983. This is the first observation of the intermolecular rearrangement reaction in a weakly bound binary complex. They have measured an action spectrum by observing the 500-nm chemiluminescence of the product HgCl and by scanning the pump wavelength in the region of the $Hg(6^3P_1) \leftarrow Hg(6^1S_0)$ tran-

sition. A single broad band is observed, whose peak is at the higher energy side of the atomic transition of Hg (the $\tilde{B} \leftarrow \tilde{X}$ region).[37,38]

In the excitation and action spectra of complexes such as Hg·(rare gas), Hg·CH_4, and Hg·N_2, progressions due to the intermolecular vibrations have been observed (see discussion above). The broad band observed here in the action spectrum is then characteristic of Hg·Cl_2 and has been attributed to the transition to $\tilde{B}^3\Sigma^+$ which is strongly mixed with a CT configuration, $Hg^+ \cdot Cl_2^-$. On the basis of these observations, the following mechanism has been proposed:[37,38]

$$Hg \cdot Cl_2 + h\nu\ (\sim 253\ nm) \rightarrow Hg^+ \cdot Cl_2^-$$

$$Hg^+ \cdot Cl_2^- \rightarrow HgCl(B^2\Sigma^+) + Cl(^2P_{1/2,3/2})$$

$$HgCl(B^2\Sigma^+) \rightarrow h\nu\ (500\ nm) + HgCl(X^2\Sigma^+) \quad (23)$$

The reaction of photoexcited $Hg(6^3P_1)$ with Cl_2 has been studied in the gas phase[97,123] and in the crossed molecular beam configuration.[124] A strikingly large cross section of the order of 100 Å^2 has been explained on the basis of the harpooning mechanism. The correlations of potential surfaces are essentially the same as those shown in Figure 11 for Ca·HCl except that the singlet spin should be read as triplet. The $^3P_1^1(^3\Sigma^+)$ state is crossed by a Σ-type CT surface, $Hg^+(^2S) + Cl_2^-(^2\Sigma^+)$ (avoided crossing), at a longer Hg–Cl_2 distance, which accounts for the extraordinarily large cross section.

Since, in view of the value of cross section, the Hg–Cl_2 distance at the crossing point may be much larger than the bond distance (~4 Å) of Hg·Cl_2 in its ground state, the excitation of the complex is presumably to the state mainly of CT character (similarly to the vertical arrow in Figure 11). This CT(Σ) surface is correlated to $HgCl(B^2\Sigma^+) + Cl(^2P)$, accounting for the observed chemiluminescence. In contrast to Ca·HCl, the HgCl(A → X) emission was not observed. Moreover, the $\tilde{A}(^3\Pi)$ state is not observed in the action spectrum obtained by monitoring the B → X transition of HgCl. These results indicate that the reaction proceeds retaining the $C_{\infty v}$ symmetry, with no avoided crossing like that at P in Figure 11. HgCl(A) is then correlated only to Hg·$Cl_2(\tilde{A})$. Jouvet et al. have ascribed the nonobservation of the Hg·$Cl_2(\tilde{A})$–HgCl(A) channel to a strong interaction of the $\tilde{A}(^3\Pi)$ state with the corresponding CT configuration which makes the state move out of the spectral region being detected.[39] It should also be noted that the HgCl(A) state may not be emissive.[125] However, in view of the surfaces like those in Figure 11, the channel $\tilde{A}$ → CT(Π) → CaCl(A) may have an activation barrier near the crossing point of $\tilde{A}$ and CT(Π). Excitation to $\tilde{A}$ would not provide sufficient energy to overcome the barrier. It would therefore be more reasonable to try to excite the CT(Π) surface directly at shorter wavelengths. Nevertheless, the direct spectroscopic observation of the CT state $Hg^+ \cdot Cl_2^-$ is good evidence for the harpooning mechanism taking place both in the reactant-pair and in the bimolecular reactions.

5. *Xe·X_2 (X = Cl, Br, and I)*

The photoassisted formation of excimers Rg·X* (Rg = rare gas, X = halogen) in collision of Rg and X_2 has been studied extensively.[99-101,126-139] The formation of XeX from reactant–pairs, Xe·X_2 (X = Cl, Br, or I), was investigated by Boivineau et al.[48,49,51] and summarized by Jouvet and Boivineau.[50]

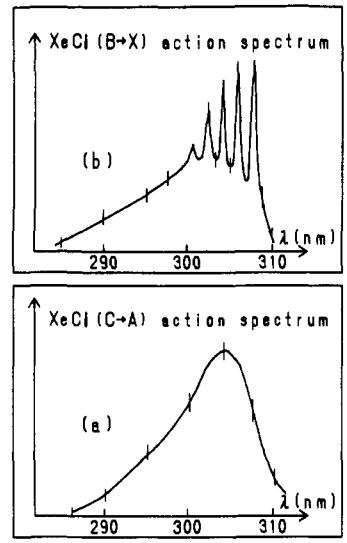

Figure 13. XeCl action spectra obtained by exciting Xe·Cl_2 with a two-photon process and by monitoring the emission of XeCl (a) at 345 nm (C state) and (b) at 308 nm (B state).[39]

Among them, the reaction of Xe·Cl_2 has been investigated most extensively. Boivineau et al.[48,49] observed two chemiluminescence bands due to the $B_{1/2} \rightarrow X_{1/2}$ and $C_{3/2} \rightarrow A_{3/2}$ transitions of XeCl* using the two-photon excitation of Xe·Cl_2 to the Rydberg state with the 297.5-nm light. On the basis of the integrated intensities of the chemiluminescence bands, they have concluded that the branching ratio into $XeCl^*(B_{1/2})$ and $XeCl^*(C_{3/2})$ is close to unity, which may be compared with the branching ratio of 1.3 obtained for the bimolecular reaction $Xe(^3P_2) + Cl_2$.[126]

XeCl* generated from Xe·Cl_2 is vibrationally cold, in constrast to the hot XeCl* generation under the bimolecular condition.[99,101,127,132] The highest vibrational levels are $v' \approx 10$ and 100 for the reactant–pair and bimolecular reactions, respectively. This difference has been discussed on the basis of the harpooning mechanism via $Xe^+ \cdot Cl_2^-$. The distance between Xe and Cl in the ground-state Xe·Cl_2 is about 3.3 Å. A Franck–Condon transition brings it directly to the $Xe^+ \cdot Cl_2^-$ surface, where XeCl* is formed, whose equilibrium bond length is also about 3 Å. Therefore, XeCl* generated from the reactant–pair is not vibrationally excited. On the other hand, in the bimolecular reaction, the Xe* + Cl_2 surface crosses the $Xe^+ + Cl_2^-$ surface at the Xe–Cl distance of about 5 Å, where the harpooning occurs. The bond length of nascent XeCl* produced from $Xe^+ \cdot Cl_2^-$ is, therefore, about 5 Å, which is much longer than the equilibrium bond length of XeCl*, resulting in a vibrationally excited XeCl*. The $Xe^+ \cdot Cl_2^-$ potential energy surface and classical trajectory calculations have been reported.[39,48]

Action spectra have been measured for XeCl*(B) and XeCl*(C) by two-photon excitation of Xe·Cl_2 in the 290–310-nm region (Figure 13).[39,49] The action spectrum measured by monitoring the $XeCl(C_{3/2} \rightarrow A_{3/2})$ fluorescence at 345 nm, shows a broad structureless band extending over 4000 cm^{-1}. It has been ascribed to the transition to a CT state $Xe^+ \cdot Cl_2^-$. In the action spectrum for the $XeCl(B_{1/2})$ formation monitored at 308

nm, vibrational structures with a spacing of 380 ± 20 cm^{-1} are observed in addition to a broad band similar to the $XeCl(C_{3/2})$ case.

The following mechanism has been proposed on the basis of the laser power saturation effect which suggests a two-step excitation via an intermediate resonant state:

$$Xe{\cdot}Cl_2 \xrightarrow{h\nu} Xe{\cdot}Cl_2(^1\Pi_u) \rightarrow XeCl(X){\cdot}Cl \xrightarrow{h\nu} XeCl(B){\cdot}Cl \rightarrow XeCl(B) + Cl \quad (24)$$

$$Xe{\cdot}Cl_2 \xrightarrow{h\nu} Xe{\cdot}Cl_2(^1\Pi_u) \xrightarrow{h\nu} Xe{\cdot}Cl_2(^1\Pi_g) \rightarrow Xe^+{\cdot}Cl_2^- \rightarrow XeCl(B,C) + Cl \quad (25)$$

where designations $^1\Pi_u$ and $^1\Pi_g$ are for the excited states of Cl_2. Since $Cl_2(^1\Pi_u)$ is a dissociative state, two processes compete at this stage, one dissociating to give XeCl·Cl and the other absorbing the second photon. The former process absorbs the second photon in the XeCl(X) part of the complex. Therefore, the structure in the action spectrum is expected to be similar to that in the LIF spectrum of XeCl(X), as has actually been observed.[49] On the other hand, the broad band in the XeCl(B) and XeCl(C) action spectra have been attributed to mechanism 25.

No structure is observed in the XeCl(B) action spectrum measured under the bimolecular condition.[99,132] This has been ascribed to an averaging over various values of impact parameter and collision energy. It has also been reported that $Xe^*(^3P_2$ or $^3P_1) + Cl_2$ gives XeCl* in a bimolecular reaction, while the excitation of $Xe{\cdot}Cl_2$ to the state correlated with $Xe^*(^3P_2$ or $^3P_1)$ does not give XeCl*. This result has been explained as due to the fact that the potential surface of $Xe^*{\cdot}Cl_2$ does not cross the XeCl* + Cl surface in the stable conformation of $Xe{\cdot}Cl_2$.

Photoexcitation of $Xe{\cdot}I_2$ does not give XeI*.[50] $Xe{\cdot}Br_2$ reacts to give XeBr* by a two-step excitation to the highly excited valence state via the B state of Br_2.[50,51] Direct two-photon excitation to the Rydberg state causes a dissociation into Xe + 2Br. The difference in the reactivity has been explained as due to the different modes of crossing between the repulsive curves and the Rydberg and valence states of halogens.[50]

IV. A Prospect of Future Developments

Finally, we give a few comments on the possible future developments in this field. As is clear in the above discussions, knowledge of the geometrical configuration of the complex is essential to analyze the dynamics of the reactant-pair reactions. Unfortunately, structural information is lacked in many cases because of the difficulty in determining structures under the molecular beam condition. However, structural data have been accumulated recently by the application of high-resolution spectroscopic techniques. More efforts are required in this direction. The structural change during the course of reaction has been postulated several times in the above discussions. The change often causes a mixing of potential energy surfaces, giving a drastic effect on the branching ratio. In order to elucidate this point, ab initio calculations would be particularly helpful in addition to the experimental examination of the state-to-state selectivity between the parent complex and products.

The dependence of the reaction cross section and branching ratio on the photolysis energy has not been studied extensively for the systems discussed in section II. Importance of the knowledge of the photolysis energy dependence has been postulated above for the discussion of $HBr{\cdot}N_2O$ in comparison with $HI{\cdot}N_2O$. More generally, it is essential to examine the excess energy dependence of the cross section to understand the reaction mechanism fully, since the reaction scheme may change according to the excess energy as discussed in section II.B.

As discussed in section II.G.3, photolysis wavelength dependence of the $HI{\cdot}CC_2$ reaction has been measured by monitoring the product LIF intensity at a fixed wavelength, indicating a monotonous increase of the cross section for increasing energy. However, this is not surprising in view of the dissociative nature of the photoexcited state. It would be more important to see how the reaction mechanism changes from direct to indirect or vice versa according to the excess energy. To accomplish this, it is necessary to measure more detailed features such as the rotational distribution, the distributions on the SO and Λ-doublet components, although a tedious experimental effort would be required to construct a two-dimensional spectrum with varying photolysis and probe wavelengths simultaneously.

In the case of excitation to the bound state discussed in section III, it is essential to find the excited states, say Ã and B̃, in the LIF or action spectrum. In the harpooning case such as Ca·HCl or $Hg{\cdot}Cl_2$, it is required to search for the Ã component [or CT(II) as discussed above] in their action spectra which has not been found so far. Some of the complexes of Hg (such as $Hg{\cdot}NH_3$, $Hg{\cdot}CH_4$, etc.) undergo only the decomposition to their constituents as mentioned above. One of the reasons for this may be insufficient excess energy to promote the rearrangement reaction between the constituent molecules. Excitation to higher excited states may open a new possibility in this type of complexes. The extended pump energy range would also make it possible to cover a wide variety of counter molecules which form complexes with Hg.

It is of particular interest to see the effect of intermolecular mode excitation. Unfortunately, few examples have been reported only for the Hg complexes. Observation of the vibronic structure due to the intermolecular vibrational modes is generally not easy because of their low frequencies which could be broadened out if the dissociation is too fast, and because of low Franck–Condon factors due to a weak coupling between the intermolecular and intramolecular vibrational modes. The Hg complexes may be an exceptional case where the direct interaction of the atomic valence electrons with the intermolecular modes enhances the coupling. Nevertheless, it is fascinating that the intermolecular mode selective chemistry has been observed in some of these complexes. A search for a similar effect in the excitation of molecular species in a complex is desired.

We have reviewed here two types of reactions in which the complex is photoexcited either to the dissociative or to the bound state. Nevertheless, very restricted types of complexes have been studied so far. In the former case, most of the reactions studied are those which produce the OH radical, presumably because of its feasibleness in optical detection and well-known spectroscopic characteristics. It is, however,

necessary to extend the detection to other species in order to establish characteristic features of the complex-initiated dynamics.

In the case of the excitation to the bound states, a variety of examples reported for the bimolecular mercury-sensitized reactions,[97] which would give us additional possibilities for studying the reactant-pair reactions with Hg. For example, various alkanes, RH, have been reported to undergo the mercury-sensitized bimolecular reaction to form $HgH(X^2\Sigma^+)$.[97,140] The bimolecular reactions using other metal atoms such as Zn and Cd have also been reported, which suggests the possibility of studying them in the reactant-pair reaction.[46,97] A systematic search for such combinations is required.

Perhaps one of the advantages of using the atomic species for the photoexcitation is that most of the excitation energy can be used to dissociate the counter molecule. If one excites the molecular species, say A–B in complex A–B·C–D, most of the photon energy is consumed to break the A–B bond, only the residual energy being used to dissociate C–D. If (A–B)* is a dissociative state, the activation barrier must be relatively lower for (A–B)*·C–D → A + B–C + D so that this reaction may be possible for a relatively weak C–D bond. This is the case for the complexes discussed in section II. When (A–B)* is a bound state, the activation barrier should be higher and the residual energy in the near UV excitation can hardly overcome it. It is perhaps possible to study a complex (A–B)*·C–D where (A–B)* is a predissociative excited state. In this case, the effective activation barrier is expected to be lower than the purely bound state, which could be overcome by a single-photon excitation in the UV region. This possibility should also be examined in the future.

References

(1) Harland, P. W.; Carman, H. S., Jr.; Phillips, L. F.; Brooks, P. R. *J. Chem. Phys.* **1990**, *93*, 1089.
(2) Parker, D. H.; Bernstein, R. B. *Ann. Rev. Phys. Chem.* **1989**, *40*, 561.
(3) Jalink, H.; Nicolasen, G.; Stolte, S.; Parker, D. H. *J. Chem. Soc., Faraday Trans. 2* **1989**, *85*, 1115 (special issue on "Orientation and Polarization Effects in Reactive Collisions").
(4) Ohoyama, H.; Kasai, T.; Ohashi, K.; Kuwata, K. *Chem. Phys. Lett.* **1987**, *136*, 236.
(5) Stolte, S. *Ber. Bunsen-Ges. Phys. Chem.* **1982**, *86*, 413.
(6) Leone, S. R. *Ann. Rev. Phys. Chem.* **1984**, *35*, 109.
(7) Leone, S. R. *Phys. Today* **1987**, S-11.
(8) Bernstein, R. B.; Herschbach, D. R.; Levine, R. D. *J. Phys. Chem.* **1987**, *87*, 5365 (special issue on "Dynamical Stereochemistry").
(9) Suits, A. G.; Hou, H.; Lee, Y. T. *J. Phys. Chem.* **1990**, *94*, 5672.
(10) Hoffmeister, M.; Schleysing, R.; Loesch, H. *J. Phys. Chem.* **1987**, *91*, 5441.
(11) deVries, M. S.; Tyndall, G. W.; Cobb, C. L.; Martin, R. M. *J. Chem. Phys.* **1987**, *86*, 2653.
(12) Leone, S. R. *Science* **1985**, *227*, 889.
(13) Rettner, C. T.; Zare, R. N. *J. Chem. Phys.* **1982**, *77*, 2416.
(14) Rettner, C. T.; Zare, R. N. *J. Chem. Phys.* **1981**, *75*, 3636.
(15) Van Den Meijdenberg, C. J. N. In *Atomic and Molecular Beam Methods*; Scoles, G.; Ed.; Oxford University Press: New York, 1988; p 345.
(16) Honma, K.; Kajimoto, O. *Chem. Phys. Lett.* **1985**, *117*, 123.
(17) Honma, K.; Fujimura, Y.; Kajimoto, O.; Inoue, G. *J. Chem. Phys.* **1988**, *88*, 4739.
(18) Buelow, S.; Radhakrishnan, G.; Catanzarite, J.; Wittig, C. *J. Chem. Phys.* **1985**, *83*, 444.
(19) Radhakrishnan, G.; Buelow, S.; Wittig, C. *J. Chem. Phys.* **1986**, *84*, 727.
(20) Wittig, C.; Engel, Y. M.; Levine, R. D. *Chem. Phys. Lett.* **1988**, *153*, 411.
(21) Wittig, C.; Hoffmann, G.; Chen, Y.; Iams, H.; Oh, D. *J. Chem. Soc., Faraday Trans 2* **1989**, *85*, 1292.
(22) Schatz, G. C.; Fitzcharles, M. S. In *Selectivity in Chemical Reactions*; Whitehead, J. C., Ed.; Kluwer Academic Publishers: Dordrecht, 1988; p 353.
(23) Buelow, S.; Radhakrishnan, G.; Wittig, C. *J. Phys. Chem.* **1987**, *91*, 5409.
(24) Scherer, N. F.; Khundkar, L. R.; Bernstein, R. B.; Zewail, A. H. *J. Chem. Phys.* **1987**, *87*, 1451.
(25) Scherer, N. F.; Sipes, C.; Bernstein, R. B.; Zewail, A. H. *J. Chem. Phys.* **1990**, *92*, 5239.
(26) Chen, Y.; Hoffmann, G.; Oh, D.; Wittig, C. *Chem. Phys. Lett.* **1989**, *159*, 426.
(27) Hoffmann, C.; Oh, D.; Chen, Y.; Engel, Y. M.; Wittig, C. *Israel J. Chem.* **1990**, *30*, 115.
(28) Haeusler, D.; Rice, J.; Wittig, C. *J. Phys. Chem.* **1987**, *91*, 5413.
(29) Rice, J.; Hoffmann, G.; Wittig, C. *J. Chem. Phys.* **1988**, *88*, 2841.
(30) Hoffmann, G.; Oh, D.; Iams, H.; Wittig, C. *Chem. Phys. Lett.* **1989**, *155*, 356.
(31) Hoffmann, G.; Oh, D.; Wittig, C. *J. Chem. Soc., Faraday Trans. 2* **1989**, *85*, 1141.
(32) (a) Ohoyama, H.; Takayanagi, M.; Nishiya, T.; Hanazaki, I. *Chem. Phys. Lett.* **1989**, *162*, 1. (b) Ohoyama, H.; Takayanagi, M.; Nishiya, T.; Hanazaki, I. To be published.
(33) Sivakumar, N.; Burak, I.; Cheung, W.-Y.; Houston, P. L.; Hepburn, J. W. *J. Phys. Chem.* **1985**, *89*, 3609.
(34) Sivakumar, N.; Hall, G. E.; Houston, P. L.; Hepburn, J. W.; Burak, I. *J. Chem. Phys.* **1988**, *88*, 3692.
(35) Buelow, S.; Noble, M.; Radhakrishnan, G.; Reisler, H.; Wittig, C.; Hancock, G. *J. Phys. Chem.* **1986**, *90*, 1015.
(36) Wittig, C.; Sharpe, S.; Beaudet, R. A. *Acc. Chem. Res.* **1988**, *21*, 341.
(37) Jouvet, C.; Soep, B. *Chem. Phys. Lett.* **1983**, *96*, 426.
(38) Jouvet, C.; Soep, B. *J. Phys., Colloq.* **1985**, *46*, C1-313.
(39) Jouvet, C.; Boivineau, M.; Duval, M. C.; Soep, B. *J. Phys. Chem.* **1987**, *91*, 5416.
(40) Jouvet, C.; Soep, B. *Laser Chem.* **1985**, *5*, 157.
(41) Jouvet, C.; Boivineau, M.; Duval, M. C.; Soep, B. *Phys. Scr.* **1988**, *T23*, 155.
(42) Jouvet, C.; Duval, M. C.; Soep, B.; Breckenridge, W. H.; Whitham, C.; Visticot, J. P. *J. Chem. Soc., Faraday Trans. 2* **1989**, *85*, 1133.
(43) Breckenridge, W. H.; Jouvet, C.; Soep, B. *J. Chem. Phys.* **1986**, *84*, 1443.
(44) Breckenridge, W. H.; Duval, M. C.; Jouvet, C.; Soep, B. *J. Chim. Phys.-Chim. Biol.* **1987**, *84*, 381.
(45) Breckenridge, W. H.; Benoist d'Azy, O.; Duval, M. C.; Jouvet, C.; Soep, B. In *Stochasticity and Intermolecular Redistribution of Energy*; Lefebvre, R., Mukamel, S., Ed.; D. Reidel Publishing Company: Dordrecht, 1987; p 149.
(46) Breckenridge, W. H. *Acc. Chem. Res.* **1989**, *22*, 21.
(47) Bernier, A.; Millie, P. *J. Chem. Phys.* **1988**, *88*, 4843.
(48) Boivineau, M.; Le Calve, J.; Castex, M. C.; Jouvet, C. *Chem. Phys. Lett.* **1986**, *128*, 528.
(49) Boivineau, M.; Le Calve, J.; Castex, M. C.; Jouvet, C. *Chem. Phys. Lett.* **1986**, *130*, 208.
(50) Jouvet, C.; Boivineau, M. In *Selectivity in Chemical Reactions*; Whitehead, J. C., Ed.; Kluwer Academic Publishers: Dordrecht, 1988; p 341.
(51) Boivineau, M.; Le Calve, J.; Castex, M.-C.; Jouvet, C. *J. Chem. Phys.* **1986**, *84*, 4712.
(52) Visticot, J. P.; Soep, B.; Whitham, C. J. *J. Phys. Chem.* **1988**, *92*, 4574.
(53) Visticot, J. P.; Keller, A.; Witham, C.; Soep, B. *J. Chem. Soc., Faraday Trans. 2* **1989**, *85*, 1289.
(54) Jouvet, C.; Beswick, J. A. *J. Chem. Phys.* **1987**, *86*, 5500.
(55) Jouvet, C.; Soep, B. *J. Chem. Phys.* **1984**, *80*, 2229.
(56) Fuke, K.; Saito, T.; Nonose, S.; Kaya, K. *J. Chem. Phys.* **1987**, *86*, 4745.
(57) Breckenridge, W. H.; Duval, M. C.; Jouvet, C.; Soep, B. In *Structure and Dynamics of Weakly Bound Molecular Complexes*; Weber, A., Ed.; D. Reidel Publishing Company: Dordrecht, 1987; p 213.
(58) Yamanouchi, K.; Isogai, S.; Tsuchiya, S.; Duval, M.-C.; Jouvet, C.; Benoist d'Azy, O.; Soep, B. *J. Chem. Phys.* **1988**, *89*, 2975.
(59) Duval, M.-C.; Soep, B. *Chem. Phys. Lett.* **1987**, *141*, 225.
(60) van Zee, R.; Bosma, W. B.; Zwier, T.; Duval, M.-C.; Soep, B. *Jerusalem Symp. Quantum Chem. Biochem.* **1987**, *20*, 101.
(61) Duval, M. C.; Soep, B.; van Zee, R. D.; Bosma, W. B.; Zwier, T. S. *J. Chem. Phys.* **1988**, *88*, 2148.
(62) Celii, F. G.; Janda, K. C. *Chem. Rev.* **1986**, *86*, 507.
(63) Miller, R. E. *J. Phys. Chem.* **1986**, *90*, 3301.
(64) Tzeng, W.-B.; Ono, Y.; Linn, S. H.; Ng, C. Y. *J. Chem. Phys.* **1985**, *83*, 2803 and references cited therein.
(65) Tzeng, W.-B.; Ono, Y.; Linn, S. H.; Ng, C. Y. *J. Chem. Phys.* **1985**, *83*, 2813 and references cited therein.
(66) Castleman, A. W., Jr.; Keesee, R. G. *Chem. Rev.* **1986**, *86*, 589.
(67) Joyner, C. H.; Dixon, T. A.; Baiocchi, F. A.; Klemperer, W. *J. Chem. Phys.* **1981**, *74*, 6550.

(68) Andrews, L.; Johnson, G. L. *J. Chem. Phys.* **1982**, *76*, 2875.
(69) Lovejoy, C. M.; Nesbitt, D. J. *J. Chem. Phys.* **1987**, *87*, 1450.
(70) Kukolich, S. G.; Bumgarner, R. E.; Pauley, D. J. *Chem. Phys. Lett.* **1987**, *141*, 12.
(71) Dayton, D. C.; Miller, R. E. *Chem. Phys. Lett.* **1988**, *143*, 580.
(72) Andrews, L.; Bohn, R. B.; Arlinghaus, R. T.; Hunt, R. D. *Chem. Phys. Lett.* **1989**, *158*, 564.
(73) (a) Kukolich, S. G.; Pauley, D. J. *Chem. Phys.* **1989**, *131*, 403. (b) Kukolich, S. G.; Pauley, D. J. *Chem. Phys.* **1989**, *135*, 161.
(74) (a) Kukolich, S. G.; Pauley, D. J. *J. Chem. Phys.* **1989**, *90*, 3458. (b) Kukolich, S. G.; Pauley, D. J. *J. Chem. Phys.* **1990**, *93*, 1487.
(75) Lovejoy, C. M.; Nesbitt, D. J. *J. Chem. Phys.* **1989**, *90*, 4671.
(76) Zeng, Y. P.; Sharpe, S. W.; Reifschneider, D.; Wittig, C.; Beaudet, R. A. *J. Chem. Phys.* **1990**, *93*, 183.
(77) Marshall, P.; Fontijn, A.; Melius, C. F. *J. Chem. Phys.* **1987**, *86*, 5540.
(78) Herzberg, G. *Spectra of Diatomic Molecules*, 2nd ed.; Van Nostrand: Princeton, 1968.
(79) Alexander, M. H.; Andresen, P.; Bacis, R.; Bersohn, R.; Comes, F. J.; Dagdigian, P. J.; Dixon, R. N.; Field, R. W.; Flynn, G. W.; Gericke, K.-H.; Grant, E. R.; Howard, B. J.; Huber, J. R.; King, D. S.; Kinsey, J. L.; Kleinermanns, K.; Kuchitu, K.; Luntz, A. C.; McCaffery, A. J.; Pouilly, B.; Reisler, H.; Rosenwaks, S.; Rothe, E. W.; Shapiro, M.; Simons, J. P.; Vasudev, R.; Wiesenfeld, J. R.; Wittig, C.; Zare, R. N. *J. Chem. Phys.* **1988**, *89*, 1749.
(80) Clyne, M. A. A.; Coxon, J. A.; Woon Fat, A. R. *J. Mol. Spectrosc.* **1973**, *46*, 146.
(81) Dimpfl, W. L.; Kinsey, J. L. *J. Quant. Radiat. Transfer* **1979**, *21*, 233.
(82) Chidsey, I. L.; Crosley, D. R. *J. Quant. Radiat. Transfer* **1980**, *23*, 187.
(83) Clear, R. D.; Riley, S. J.; Wilson, K. R. *J. Chem. Phys.* **1975**, *63*, 1340.
(84) Baiocchi, F. A.; Dixon, T. A.; Joyner, C. H.; Klemperer, W. *J. Chem. Phys.* **1981**, *74*, 6544.
(85) Shea, J. A.; Read, W. G.; Campbell, E. J. *J. Chem. Phys.* **1983**, *79*, 614.
(86) Lovejoy, C. M.; Schuder, M. D.; Nesbitt, D. J. *J. Chem. Phys.* **1987**, *86*, 5337.
(87) Fraser, G. T.; Pine, A. S.; Suenram, R. D.; Dayton, D. C.; Miller, R. E. *J. Chem. Phys.* **1989**, *90*, 1330.
(88) Sharpe, S. W.; Zeng, Y. P.; Wittig, C.; Beaudet, R. A. *J. Chem. Phys.* **1990**, *92*, 943.
(89) Altman, R. S.; Marshall, M. D.; Klemperer, W. *J. Chem. Phys.* **1982**, *77*, 4344.
(90) Rice, J. K.; Coudert, L. H.; Matsumura, K.; Suenram, R. D.; Lovas, F. J.; Stahl, W.; Pauley, D. J.; Kukolich, S. G. *J. Chem. Phys.* **1990**, *92*, 6408.
(91) Legon, A. C.; Willoughby, L. C. *J. Mol. Struct.* **1985**, *131*, 159.
(92) Ohshima, Y.; Matsumoto, Y.; Takami, M.; Kuchitu, K. *Chem. Phys. Lett.* **1988**, *152*, 294.
(93) Huang, Z. S.; Miller, R. E. *J. Chem. Phys.* **1988**, *89*, 5408.
(94) Quick, C. R., Jr.; Tiee, J. J. *Chem. Phys. Lett.* **1983**, *100*, 223 and references cited therein.
(95) Tiee, J. J.; Ferris, M. J.; Wampler, F. B. *J. Chem. Phys.* **1983**, *79*, 130.
(96) Friedl, R. R.; Brune, W. H.; Anderson, J. G. *J. Chem. Phys.* **1983**, *79*, 4227.
(97) Breckenridge, W. H.; Umemoto, H. *Adv. Chem. Phys.* **1982**, *50*, 325.
(98) Callear, A. B. *Chem. Rev.* **1987**, *87*, 335.
(99) Setser, D. W.; Ku, J. In *Photophysics and Photochemistry above 6 eV*; Lahmani, F., Ed.; Elsevier Science Publishers B. V.: Amsterdam, 1985, p 621.
(100) Yu, Y. C.; Setser, D. W.; Horiguchi, H. *J. Phys. Chem.* **1983**, *87*, 2199 and references cited therein.
(101) Tamagake, K.; Kolts, J. H.; Setser, D. W. *J. Chem. Phys.* **1979**, *71*, 1264 and references cited therein.
(102) Duval, M.-C.; Jouvet, C.; Soep, B. *Chem. Phys. Lett.* **1985**, *119*, 317.
(103) Breckenridge, W. H.; Duval, M.-C.; Jouvet, C.; Soep, B. *Chem. Phys. Lett.* **1985**, *122*, 181.
(104) Lam, L. K.; Gallagher, A.; Drullinger, R. *J. Chem. Phys.* **1978**, *68*, 4411.
(105) Fuke, K.; Saito, T.; Kaya, K. *J. Chem. Phys.* **1983**, *79*, 2487.
(106) Fuke, K.; Saito, T.; Kaya, K. *J. Chem. Phys.* **1984**, *81*, 2591.
(107) Fuke, K.; Nonose, S.; Kaya, K. *J. Chem. Phys.* **1986**, *85*, 1696.
(108) Yamanouchi, K.; Fukuyama, H.; Horiguchi, H.; Tsuchiya, S.; Fuke, K.; Saito, T.; Kaya, K. *J. Chem. Phys.* **1986**, *85*, 1806.
(109) Duval, M.-C.; Benoist d'Azy, O.; Breckenridge, W. H.; Jouvet, C.; Soep, B. *J. Chem. Phys.* **1986**, *85*, 6324.
(110) Yamanouchi, K.; Isogai, S.; Okunishi, M.; Tsuchiya, S. *J. Chem. Phys.* **1988**, *88*, 205.
(111) Polany, M. *Atomic Reactions*; Williams and Norgate: London, 1932.
(112) Weiner, J. *J. Chem. Phys.* **1980**, *72*, 5731.
(113) Smalley, R. E. *Laser Chem.* **1983**, *2*, 167.
(114) Adams, N.; Breckenridge, W. H.; Simons, J. *Chem. Phys.* **1981**, *56*, 327.
(115) Blickensderfer, R. P.; Jordan, K. D.; Adams, N.; Breckenridge, W. H. *J. Phys. Chem.* **1982**, *86*, 1930.
(116) Poirier, R. A.; Peterson, M. R.; Menzinger, M. *J. Chem. Phys.* **1983**, *78*, 4592.
(117) Chaquin, P.; Sevin, A.; Yu, H. *J. Phys. Chem.* **1985**, *89*, 2813.
(118) Horiguchi, H.; Tsuchiya, S. *Bull. Chem. Soc. Jpn.* **1974**, *47*, 2768.
(119) Horiguchi, H.; Tsuchiya, S. *Bull. Chem. Soc. Jpn.* **1977**, *50*, 1657.
(120) Brinkmann, U.; Telle, H. *J. Phys. B* **1977**, *10*, 133.
(121) Telle, H.; Brinkmann, U. *Mol. Phys.* **1980**, *39*, 361.
(122) Brinkmann, U.; Schmidt, V. H.; Telle, H. *Chem. Phys. Lett.* **1980**, *73*, 530.
(123) Dreiling, T. D.; Setser, D. W. *J. Chem. Phys.* **1983**, *79*, 5423.
(124) Krause, H. F.; Johnson, S. G.; Datz, S.; Schmidt-Bleek, F. K. *Chem. Phys. Lett.* **1975**, *31*, 577.
(125) Huber, K. P.; Herzberg, G. *Molecular Spectra and Molecular Structure IV. Constants of Diatomic Molecules*; van Nostrand Reinhold: New York, 1979.
(126) Velazco, J. F.; Kolts, J. H.; Setser, D. W. *J. Chem. Phys.* **1976**, *65*, 3468.
(127) Brashears, H. C., Jr.; Setser, D. W. *J. Phys. Chem.* **1980**, *84*, 224.
(128) Grieneisen, H. P.; Xue-Jing, H.; Kompa, K. L. *Chem. Phys. Lett.* **1981**, *82*, 421.
(129) Dubov, V. S.; Lapsker, Y. E.; Samoilova, A. N.; Gurvich, L. V. *Chem. Phys. Lett.* **1981**, *83*, 518.
(130) Wilcomb, B. E.; Burnham, R. *J. Chem. Phys.* **1981**, *74*, 6784.
(131) Dreiling, T. D.; Setser, D. W. *J. Chem. Phys.* **1981**, *75*, 4360.
(132) Ku, J. K.; Inoue, G.; Setser, D. W. *J. Phys. Chem.* **1983**, *87*, 2989.
(133) Ishiwata, T.; Tokunaga, A.; Tanaka, I. *Chem. Phys. Lett.* **1984**, *112*, 356.
(134) Inoue, G.; Ku, J. K.; Setser, D. W. *J. Chem. Phys.* **1984**, *80*, 6006.
(135) O'Grady, B. V.; Donovan, R. J. *Chem. Phys. Lett.* **1985**, *122*, 503.
(136) Le Calve, J.; Castex, M. C.; Jordan, B.; Zimmerer, G.; Moeller, T.; Haaks, D. In *Photophysics and Photochemistry above 6 eV*; Lahmani, F., Ed.; Elsevier Science Publishers B. V.: Amsterdam, 1985; p 639.
(137) Wilkinson, J. P. T.; Kerr, E. A.; Lawley, K. P.; Donovan, R. J.; Shaw, D.; Hopkirk, A.; Munro, I. *Chem. Phys. Lett.* **1986**, *130*, 213.
(138) Johnson, K.; Pease, R.; Simons, J. P.; Smith, P. A.; Kvaran, A. *J. Chem. Soc., Faraday Trans. 2* **1986**, *82*, 1281.
(139) Johnson, K.; Simons, J. P.; Smith, P. A.; Kvaran, A. *J. Chim. Phys.* **1987**, *84*, 371.
(140) Vikis, A. C.; Le Roy, D. J. *Can. J. Chem.* **1973**, *51*, 1207.